Applied Thermal Engineering 244 (2024) 122610

Contents lists available at ScienceDirect

Applied Thermal Engineering

journal homepage: www.elsevier.com/locate/apthermeng

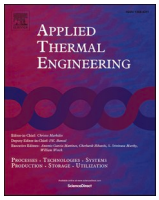

Research Paper

Thermal performance of an advanced smart fenestration systems for low-energy buildings

Yang Ming [a,*], Yanyi Sun [a,b], Xin Liu [a], Xiao Liu [a], Yupeng Wu [a,*]

[a] Faculty of Engineering, University of Nottingham, Nottingham NG7 2RD, UK
[b] Department of Civil Engineering, Surveying and Construction Management, School of Built Environment and Geography, Faculty of Engineering, Computing and the Environment, Kingston University, United Kingdom

ARTICLE INFO

Keywords:
Adaptive façade
Thermotropic material
Transparent insulation materials
Solar energy
Thermal performance

ABSTRACT

Windows significantly influence a building's indoor environment and energy consumption due to their high optical transmittance and low thermal resistance comparing with walls, affecting both indoor daylight comfort and heat gain or loss. Thermotropic (TT) materials can offer dynamic regulation of solar energy, improving building energy efficiency. Parallel slats transparent insulation materials (PS-TIM) integrated into the air cavity of double-glazing windows can effectively increase the thermal resistance of a window. In this study, these two advanced technologies were combined to develop a new type of adaptive fenestration system, named Thermotropic Parallel Slat Transparent Insulation Material (TT PS-TIM) system. The selected TT hydrogel, 5 wt% poly(N-isopropyl acrylamide) (PNIPAm), was sandwiched within polymethyl methacrylate (PMMA) slices. The slats were subsequently proposed between two glass panes to form a parallel slat transparent insulation materials system. To investigate the thermal and optical properties of the TT slats as well as the thermal performance (i.e., solar heat gain coefficient, and dynamic thermal performance in summer and winter) of the TT PS-TIM system with different slats intervals, a novel model combining Ray-tracing technique and Computational Fluid Dynamics (CFD) has been proposed. The findings of this study reveal that a TT PS-TIM system incorporating 5 wt% PNIPAm slats can offer a substantial reduction (up to 0.5) in solar transmittance as it transitions from a clear to a translucent state. Accompanied with the phase transition of the TT slats, there is a significant reduction in the Solar Heat Gain Coefficient (SHGC) of the window system. This effectively decreases the unwanted solar heat gain, thus improving the overall buildings thermal performance. According to the advanced transient simulation results based on the weather conditions of London, the TT PS-TIM system exhibits superior performance evidenced by over a 30% reduction in heat gain during summer and approximately a 20% reduction in heat loss during winter in contrast to a conventional Double Glazing (DG) system. This is evident in the form of reduced heat gain during summer and minimized heat loss during winter, resulting in a more thermally balanced environment throughout the year. The comprehensive thermal investigation of TT PS-TIM can effectively help to increase the accuracy of the further energy and daylight analysis.

1. Introduction

Buildings' energy consumption accounts for approximately 40 % of the total energy use of the world [1]. Several low-energy buildings have been developed and investigated, and advanced window is one of the low-energy building strategies, especially needed for modern architecture with large glazing coverage. As a part of the envelope, windows significantly influence not only a building's energy consumption but also indoor environment[2,3] due to their high optical transmittance and low thermal resistance, affecting both heat gain or loss and indoor daylight comfort [4,5]. Over the past decades, the demand for comfortable indoor environments has been steadily increasing [6–8]. In response to this need, smart switchable windows have emerged as a revolutionary solution. These windows possess a remarkable ability to intelligently control the transmission and reflection of light, thereby effectively minimizing heat gain and loss through the building envelope [9,10]. Smart windows adapt to indoor requirements by responding to the external environment [11]. They can be classified into four types: gasochromic, electrochromic, photochromic, and thermochromic glazing [10]. The gasochromic and electrochromic, are active technologies as they can be controlled by users. The photochromic and

* Corresponding authors.
E-mail addresses: Yang.Ming@nottingham.ac.uk (Y. Ming), Yupeng.Wu@nottingham.ac.uk (Y. Wu).

https://doi.org/10.1016/j.applthermaleng.2024.122610
Received 25 August 2023; Received in revised form 30 November 2023; Accepted 29 January 2024
Available online 3 February 2024

Nomenclature

TIM	Transparent Insulation Material
PMMA	polymethyl methacrylate
PS-TIM	parallel-slat TIM
TT	thermotropic
PNIPAm	poly(N-isopropylacrylamide)
τ_{total}	direct transmission of the solar radiation flux
α_i	solar radiation absorbed by different components of the window system
N	inward-flowing fraction
δq_{in}	heat flux difference between the situation with and without solar radiation (W/m^2)
I	solar irradiance that incident on the window surface (W/m^2)
Nu	Nusselt number
h	convective heat transfer coefficient of the flow (W/m^2·K)
L	characteristic length (m)
k	thermal conductivity of the fluid (W/m·K)
Re	Reynolds number
Pr	Prandtl number
Gr	Grashof number
ρ	density of the fluid (kg/m^3)
u	flow speed (m/s)
μ	dynamic viscosity of the fluid (kg/m·s)
g	gravitational acceleration due to Earth (m/s^2)
β	coefficient of thermal expansion (1/K)
T_{si}	surface temperature (K)
T_{ai}	bulk temperature (K)
L	vertical length (m)
ν	kinematic viscosity (m^2/s)

thermochromic, are categorised as passive technologies, which means they respond to environmental stimuli without human intervention [12,13]. Among these, thermochromic glazing has garnered significant interest. This technology integrates a layer of thermochromic or thermotropic material that modulates near-infrared (NIR) light transmittance while maintaining visible light transmittance [14]. On the other hand, it's relatively simple to produce [15,16], has lower costs [17,18], provides an ideal balance of thermal and daylight environments [19], and makes a significant contribution to energy savings [20,21]. Additionally, like photochromic windows, it is purely materials-driven and does not require additional control systems [22]. Thermotropic (TT) hydrogels like poly(N-isopropyl acrylamide) (PNIPAm) and hydroxypropyl cellulose (HPC) are of particular interest. Characterised by a reversible sol–gel phase transition responsive to temperature changes, they hold promise for thermotropic smart window systems [23,24]. Above their phase transition temperature, these hydrogels change from a transparent and solvent-swollen hydrophilic state to an opaque, highly dehydrated, and extremely hydrophobic state [25]. In this opaque or translucent state, incident visible light and solar heat are significantly blocked. Some researchers also found that the thermotropic material can offer a significant impact on solar absorption when it transits from a clear state to a translucent state [26–28]. Takashi et al., [29] developed a thermotropic glass window system for solar and daylighting control. The results show that the temperature of the window surface in a translucent state was higher than it is in a clear state which indicates its higher solar absorption in the translucent state. Haruo [30] developed a new type of thermotropic smart window and measured its spectral optical properties. It was found that the absorptance of the sample significantly increased when it transitioned from a clear to a translucent state. This high absorption property could potentially allow for effective solar energy regulation when integrated into window systems. However, despite their potential benefits in energy saving and comfort enhancement, thermotropic windows have limitation, such as obstructing occupants' view and limiting access to natural daylight when in their translucent state. This reduction in natural daylight can result in suboptimal indoor lighting conditions, necessitating the use of artificial lighting, which may compromise indoor daylight comfort and negate the intended energy savings. Furthermore, the lack of a visual connection to the outdoors can diminish occupant satisfaction. Additionally, the thermotropic windows do not improve the thermal resistance of the system, which is a critical factor in overall energy efficiency.

To address these shortcomings, integration of Thermotropic (TT) materials with Transparent Insulation Materials (TIM) in glazing systems is a novel approach to maintain the unobstructed view to the outside/inside of buildings while regulating the incident solar radiation. Additionally, a double glazing window system integrated with a TIM in a specific geometric structure such as glazing-parallel structure, glazing-perpendicular structure or cavity structure [31–36], can effectively decrease the internal convective heat transfer [37,38]. Meanwhile, the TIMs such as polymethyl methacrylate (PMMA), polyethylene (TPX), and polytetrafluorethylene (HFL) [33,35,39], has low thermal conductivity (<0.5 W/ m·K) and can offer the additional benefit of reducing unwanted conductive heat transfer through the glazing system, thereby lowering the cooling and heating loads of buildings [31,37,40]. From the plethora of geometric configurations, the Parallel-Slat TIM (PS-TIM) structure warrants special attention due to its negligible impact on visual transparency, thus maintaining an acceptable optical view [38,41]. The synergistic fusion of TT materials and TIM within this structure not only optimizes the thermal performance of the window system but also strikes an efficient balance in solar energy management and visual clarity preservation.

In recent years, only a few studies investigated this complex window system integrated with TT materials and TIM. Ming et, al., [42] optically characterised the window system applied with parallel TT TIM slat based on the experimental measurement which showcased its significant increase of absorption and notable reduction of transmittance. Sun et al., [2,40] theoretically investigated the energy performance of building applied with TT PS-TIM windows by using EnergyPlus and daylight comfort by employing RADIANCE based on annual dynamic state predicted from EnergyPlus based on the assumed optical properties. The results indicated the high potential of TT PS-TIM for energy saving and daylight comfort improvement compared with traditional double-glazed systems. However, in EnergyPlus, due to the model limitation, only equivalent layers can be used for model development which means that only glass surface temperature can be used to obtain the clear/translucent state of the system instead of the TT slat surface temperature. On the other hand, the dynamic state of TT PS-TIM has a significant impact on the energy and daylight performance as it showcased remarkable difference of solar energy block and absorption under clear and translucent state [42]. The solar absorption has a significant effect on the surface temperature of the slat showcasing quite surface temperature difference compared with glass. The previous research with simplified model and assumptions can be used for the initial design of the system. To improve the reliability of further energy and daylight performance prediction investigation, more comprehensive thermal investigation needs to be undertaken.

The integration of TT and TIM techniques precipitates an increased complexity within fenestration system designs. Based on the literature review, numerous studies have explored the thermal performance of smart fenestration systems using both numerical and experimental approaches [18,43–48]. Notably, Computational Fluid Dynamics (CFD)

has emerged as a beneficial numerical method for evaluating the thermal properties of windows due to its robust computational capabilities [49,50]. When conducting numerical analyses on the thermal performance of complex smart fenestration systems incorporating high solar absorption materials, the absorption of solar radiation becomes a significant factor to consider. For instance, Jin et al., [51] crafted an adaptive glazing system combining thermochromic glazing and phase-change materials (PCM), and scrutinized its thermal performance using CFD simulation. They ingeniously represented the solar radiation absorption, calculated by equations, as heat sources within the glazing panes and the PCM. Similarly, Xaman et al., [52] developed a room with a double glazing window system incorporating a solar control film and utilized equations to investigate the solar radiation flux impacting the solar control film on the glass numerically. Demanega et al., [53] developed a Complex Fenestration System with integrated blinds model in CFD and used Radiance to achieve solar absorption. The resulting absorbed component of solar irradiation is used as input for the CFD simulations. It is crucial to note that in these studies, incident solar radiation on the exterior glass wall was assumed to be normal to the surface.

However, when formulating a complex window system laden with TT materials characterized by strong diffusion and high absorption, the system's solar absorption becomes dynamically influenced by factors such as solar irradiance, solar incident angles, and the scattering state of the TT materials. These factors are challenging to simulate directly in CFD. Moreover, the absorbed solar energy can also affect the heat transfer of the window system when the energy is released from the material. To the best of author's knowledge, the solar heat transfer of complex smart fenestration systems with high solar absorption thermotropic materials has not been fully addressed and can be further explored with the advantage of CFD method combined with its adaptive optical properties. To achieve the solar absorption of complex fenestration system, Ray-tracing technique is commonly selected [54]. For example, Zahri et al., [55] used ray-tracing tool to investigate the absorption of the solar windows with perovskite thin films. Therefore, the application of Ray-tracing can accurately determine the solar absorption of TT materials, which can then be input into CFD for a more detailed investigation of thermal performance. While the integration of Ray-tracing and Computational Fluid Dynamics (CFD) for comprehensive analysis is not entirely unprecedented, the extent of research in this area remains limited. Notably, Bush et al., [56] pioneered an innovative technique that combined surface irradiation and volumetric absorption, derived from Monte Carlo ray-tracing, with computational heat transfer models specifically designed for solar receivers. Tao et al., [50] advanced the field by developing a thermochromic window model within a CFD framework. They utilized a solar ray-tracing algorithm to accurately account for the radiation effects emanating from the sun. To solve the radiative heat transfer equation within their CFD framework, they deployed the Discrete Ordinates (DO) radiation model. Despite the remarkable progress in integrated approaches, there remains a significant research gap in their application to complex fenestration systems. For instance, studies have yet to investigate the combination of Computational Fluid Dynamics (CFD) and ray-tracing simulations for the prediction of thermal performance in systems with considerable volume scattering and high solar absorption. Simultaneously, the advent of smart complex fenestration systems, combining thermotropic (TT) materials and thermal interface materials (TIM), has brought forth unique challenges. These innovative systems, especially in their translucent state, exhibit pronounced light diffusion, significant solar absorption, and intricate internal light ray paths. Such complex characteristics necessitate the development and application of an enhanced ray-tracing technique that integrates the aspects of volume scattering and absorption to adequately understand the solar absorption capacity of these systems. Regrettably, the extant body of literature lacks an extensive exploration into this intricate domain. Therefore, the present study aims to address this research gap and contribute to the further development and refinement of the methods for analysing complex fenestration systems.

In this paper, an advanced glazing system incorporated with TIMs and TT materials as parallel slats for indoor comfort regulation has been developed. This proposed Thermotropic Parallel Slat Transparent Insulation Material (TT PS-TIM) system can effectively maximizes solar and daylight admission during the cold season, reducing the need for heating and artificial lighting. In the hot season, the system maintains a translucent state to prevent overheating from solar heat gain and high outdoor temperatures while providing sufficient daylighting and maintaining view connection. Consequently, the TT PS-TIM system offers significant energy savings in cooling and lighting compared to conventional fenestration and shading systems. To comprehensively understand the effect of TT PS-TIM on the indoor environment for further energy and daylight simulation model reliability improvement. In this study, a proper TT material was selected for TT PS-TIM development, and a novel model combining Ray-tracing and CFD was proposed for comprehensively investigating the thermal performance of this complex smart fenestration system. After that, a prototype of TT PS-TIM system was developed and tested to validate models in Ray-tracing and CFD simulation. Furthermore, the optical and thermal performance of the TT PS-TIM system were comprehensively evaluated under various TT slat intervals, enabling a thorough assessment of its effectiveness in practical applications.

2. Methodologies

As shown in Fig. 1, a research flow chart presents the systematic progression of this study including the thermotropic material selection, characterisation, and the development of a numerical simulation method. This method combines Ray-tracing and Computational Fluid Dynamics (CFD) to comprehensively evaluate the thermal and optical attributes of the proposed TT PS-TIM. Further, its consequential implications on building energy performance are discussed. The sequential workflow is listed as follows:

1) Proper TT materials selection and characterisation were conducted for the slat and TT PS-TIM system prototype development.

2) Ray-tracing tool was employed for the TT PS-TIM optical numerical model development and the solar transmittance/absorption investigation. The precision of this model was corroborated through experimental validation.

3) A complex TT PS-TIM thermal model incorporated with the effects of solar absorption, was constructed using CFD. Combined with the overall optical transmittance of the TT PS-TIM system, a comprehensive analysis of the system's thermal performance was undertaken. Key parameters, including dynamic heat gain and loss, were systematically investigated.

2.1. Selection of TT materials and development of TT PS-TIM

Thermotropic material, PNIPAm hydrogel, with a polymer concentration ratio of 5 wt% was prepared for the development of TT slats. As PNIPAm has excellent solar energy modulation performance and ideal transition temperature of about 32 ℃ which locates in the desired temperature range for window applications [57]. The preparation of TT material can be found in the previous research [42]. After that, an advanced 10 cm x 10 cm TT PS-TIM prototype was developed for the thermal and optical numerical model validation tests, as illustrated in Fig. 2. The parallel TT slats, each measuring 10 cm in length, 1.5 cm in width, and 0.15 cm in thickness (with a 1-mm-thick 5 wt% PNIPAm membrane encapsulated inside), are sandwiched between two 0.4 cm thick optical glass panes, with an interval of 1 cm between adjacent slats. Fig. 3 presents the TT PS-TIM prototype in various states.

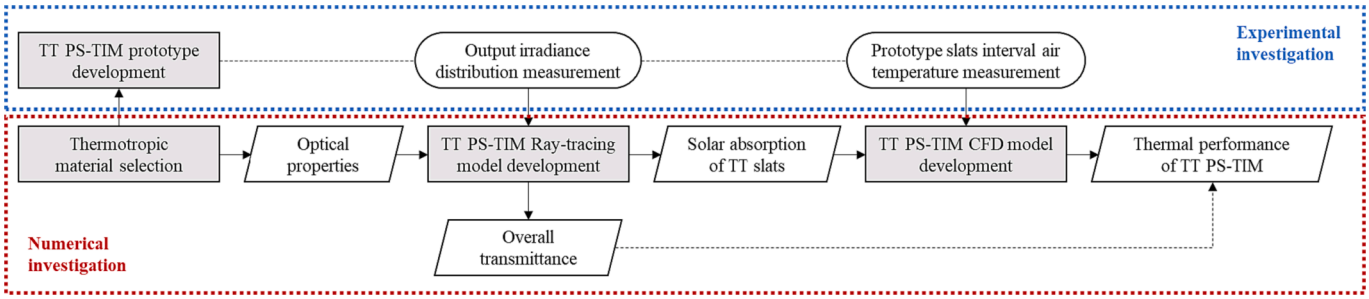

Fig. 1. Research flow chart presenting the optical and thermal model development and validation process.

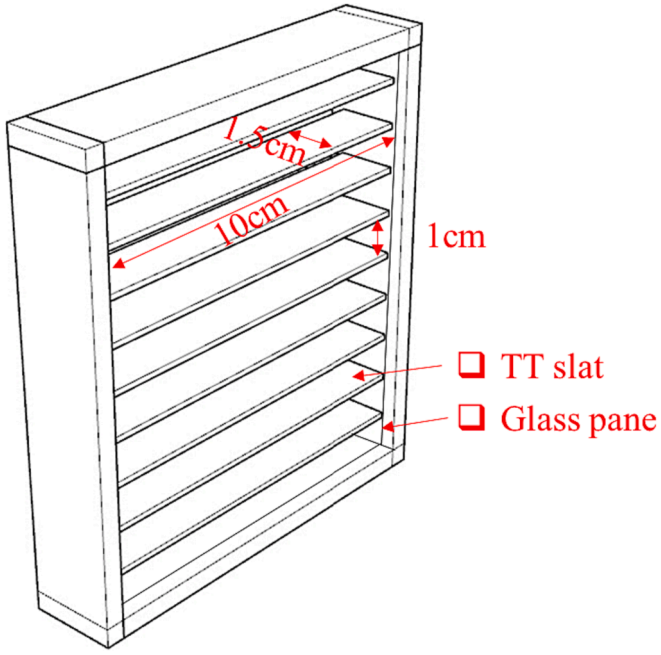

Fig. 2. TT PS-TIM system prototype.

Fig. 3. TT PS-TIM system prototype in (a) the clear state, and (b) the translucent state.

2.2. Simulation modelling of TT PS-TIM

A comprehensive understanding of the thermal performance of TT PS-TIM was achieved through the development of a novel numerical method. This novel method merges the Ray-tracing technique and Computational Fluid Dynamics (CFD) simulation methods, thereby enabling the integration of solar absorption effects into the final evaluation of the TT PS-TIM's thermal performance. This integration is exhibited as a heat released state in the thermal numerical model, which provides an avenue for an in-depth examination of the solar heat gain of the TT PS-TIM. This amalgamated approach permits a meticulous investigation into the ways that solar energy and temperature variations (indoor/outdoor) influence the behaviour of TT slats. Consequently, it aids in accurately predicting these impacts. Moreover, this method allows the simulation and analysis of the thermal behaviour of TT PS-TIM in a variety of dynamic environments.

Furthermore, the incorporation of solar energy absorption, as visualized through the heat released state in the thermal numerical model, imbues the approach with a multi-dimensional perspective that captures the interplay between the thermal properties of the TT PS-TIM and the external environmental variables. This facilitates the study of not just the thermal performance of the TT PS-TIM but also its response and adaptation to varying environmental conditions, thereby enriching the understanding of its behaviour and improving the predictive accuracy of the model.

2.2.1. Optical modelling of TT PS-TIM

For optical performance investigation, Monte-Carlo ray-tracing technique was conducted to numerically explore the optical performance of the TT PS-TIM, such as total solar transmittance, the daylight uniformity of the system and the solar absorption of each part under different solar incident angles. In ray-tracing simulation, the propagation of light rays within a model eschews any presumptions pertaining to the sequence of intersecting objects and surfaces. At each intersection, the discrete rays potentially experience a series of optical events including absorption, reflection, diffraction, and scattering. In Monte-Carlo method, the surface/medium optical properties (e. g. transmittance, reflectance and absorptance) are used as possibilities when the ray intersects the surface/medium [58,59].

In this study, a previous reported bulk scattering model [60] was used to describe the diffuse properties of the TT slats when they are in the translucent state as it can accurately simulate the light scattering occurring in the body of the thermotropic layers in the TT slats. The parameters, including scattering coefficient and anisotropy factor, can be obtained by using the inverse adding doubling (IAD) method based on the measured optical properties (e. g., total transmittance, reflectance and collimated transmittance). The detailed investigation process can be found in the previous study [42]. Fig. 4 shows the elements of the TT PS-TIM defined in the Ray-tracing model and their material optical properties used as input for the ray-tracing simulation.

In ray-tracing simulation, the model surface is fully irradiated by a virtual light source. All the materials are assumed to be optically uniform, and the directions of the incident light rays are assumed as parallel. An independent test has been conducted to determine the number of rays (>1,000,000) to launch and the flux threshold (10^{-3}) to terminate the ray tracing.

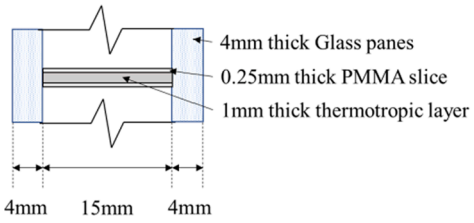

Materials	Refractive index	Absorption coefficient (mm-1)	Scattering coefficient (mm-1)	Anisotropy factor
PMMA	1.48	0.004	-	-
Glass	1.50	0.001	-	-
5 wt.% PNIPAm – clear state	1.34	0.039	-	-
5 wt.% PNIPAm – translucent state	1.34	0.173	10.60	0.76

Fig. 4. Elements in TT PS-TIM ray-tracing model and their input optical properties.

2.2.2. *Thermal modelling of TT PS-TIM*

In the context of this investigation, the well-established Computational Fluid Dynamics (CFD) software, FLUENT, was employed to develop two-dimensional models for the TT PS-TIM systems with varied TT slat intervals (i.e., 3 mm, 5 mm, 7 mm, and 10 mm). As shown in Fig. 5, the composite model includes two distinct solid constituents: a glass component exhibiting a thickness of 4 mm, and a TT slat of 1.5 mm thickness, in addition to a fluid space constituted by air. The complex simulations, encompassing this study, considered not only the fundamental thermal heat transfer, such as conduction, convection, and radiation, but also an often-overlooked element: secondary heat gains. These additional gains, induced by solar radiation absorption within the solid constituents (glass and TT slats), were accommodated by instituting heat generation boundary conditions in the simulation framework. The material properties of the air, TT slats and glass are illustrated in Table 1.

In an attempt to execute a comprehensive analysis of the thermal performance of TT PS-TIM, both steady and transient CFD models were developed and scrutinized. The steady model played a critical role in exploring the solar heat transfer capabilities, allowing for in-depth calculations of the solar heat gain coefficient (SHGC) and analysis of the critical transition boundary points of the TT PS-TIM. In contrast, the transient model was pivotal for predicting the dynamic thermal performance of the TT PS-TIM under fluctuating environmental conditions, emulating typical days within various climatic regions. In the simulation paradigm, it is assumed that the flows are steady and incompressible. It is also presumed that the flows within the cavity and cell maintain laminarity, a conclusion derived from the computed Grashof and Reynolds numbers, which are shown to be lower than their respective critical values. The upper and lower surfaces demarcating the cavity are assumed to exhibit adiabatic behaviour, and all cells within the model are assumed to be filled with air.

The establishment of boundary conditions for the outdoor and indoor glass panes, along with the TT slats in the steady simulation model, adhered to the standards delineated in ISO 15099 [61]. These boundary condition settings are listed in Table 2. The amount of solar radiation absorbed by the TT slats and glass panes was computed through the Ray-tracing simulation.

Table 1
Material thermophysical properties.

Air - Fluid	
Specific heat capacity (J/kg·K)	1005
Conductivity (W/(m·K))	0.025
Thermal expansion coefficient (1/K)	0.00353
PMMA slats – solid	
Conductivity (W/(m·K))	0.14
Emissivity	0.92
Glass panes	
Conductivity (W/(m·K))	0.94
Emissivity	0.84

Table 2
Boundary conditions for steady model simulation.

Outdoor glass	
Air temperature (°C/K)	30/303.15
Convection heat transfer coefficient (W/(m^2·K))	8
Emissivity	0.84
Outdoor glass	
Air temperature (°C/K)	25/298.15
Convection heat transfer coefficient (W/(m^2·K))	2.5
Emissivity	0.84
TT slat	
Heat generation rate (W/m^3)	Results from Ray-tracing
Emissivity	0.92

Table 3 shows the boundary conditions for the transient CFD model simulation. The outdoor and indoor glass surfaces are governed by mixed boundary conditions, a holistic framework which incorporates both thermal convective and radiative heat transfer mechanisms. To ensure the model with realistic environmental conditions, the outdoor air temperature and convection heat transfer coefficient are calibrated according to the weather data files sourced from EnergyPlus. Similarly, for the indoor environment, the mixed boundary conditions are dictated

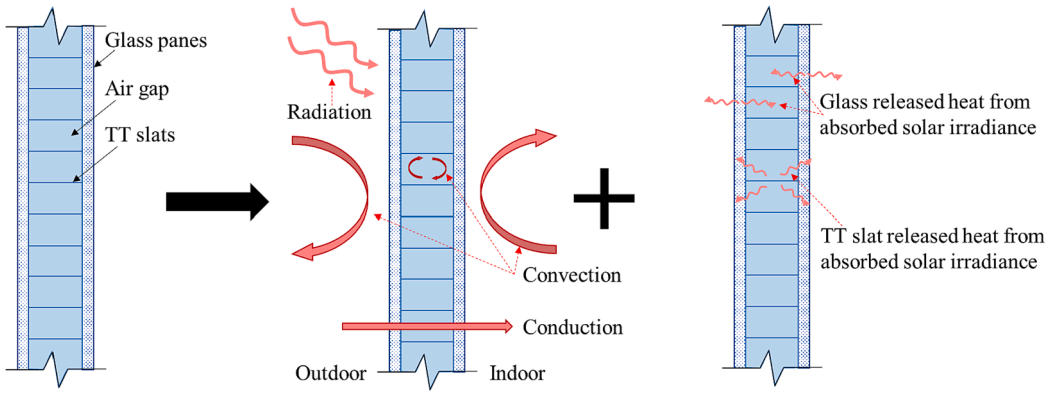

Fig. 5. TT PS-TIM numerical model development.

Table 3
Boundary conditions for transient model simulation.

Outdoor glass	
Air temperature (℃/K)	Climate weather file from EnergyPlus
Convection heat transfer coefficient (W/(m^2·K))	Climate weather file from EnergyPlus
Emissivity	0.84
Outdoor glass	
Air temperature (℃/K)	25/298.15
Convection heat transfer coefficient (W/(m^2·K))	2.5
Emissivity	0.84
TT slat	
Heat generation rate (W/m^3)	Results from Ray-tracing based on the solar irradiance in weather file
Emissivity	0.92

by the guidelines articulated in ISO 15099 [61]. The dynamism of heat generation within the TT slat is achieved by employing the Ray-tracing technique, a process that utilises solar irradiance data and incident angles, as detailed in the weather files from EnergyPlus.

To accomplish precise control over the TT slat states (clear/translucent), a User-Defined Function (UDF) was composed. When the temperature of the TT slat exceeds its transition threshold of 32℃, the state of the TT slat shifts from clear to translucent. This transition signals a significant surge in the solar absorption and heat generation rate of the TT slat in the model.

Drawing from the results obtained through the CFD simulations, the indirect solar energy transfer via the TT PS-TIM can be simulated and examined thoroughly. The influence of this indirect solar energy transfer is of substantial importance, as it significantly impacts both the indoor solar heat gain and the temperature of the TT slat. Consequently, this novel, comprehensive model facilitates the accurate prediction of the state of complex smart fenestration systems under dynamically varying outdoor environmental conditions.

Meanwhile, the calculation of the solar heat gain coefficient can be conducted, factoring in the direct transmission of solar energy through the TT PS-TIM and the indirect release of solar radiation from materials possessing high solar absorption coefficients. Consequently, the Solar Heat Gain Coefficient (SHGC) can be deduced using the following equation [62]:

$$SHGC = \tau_{total} + N\sum \alpha_i = \tau_{total} + |\delta q_{in}|/I \quad (1)$$

Where,

τ_{total} is the direct transmission of the solar radiation flux.

$N\sum\alpha_i$ is the indirect transmission of the solar radiation flux where α_i is the solar radiation absorbed by different components of the window system and N is the inward-flowing fraction.

$|\delta q_{in}|$is the heat flux difference between the situation with and without solar radiation (W/m^2), I is solar irradiance that incident on the window surface (W/m^2).

This integration of direct and indirect solar energy factors, in calculating the SHGC, provides a more comprehensive and accurate evaluation of the thermal performance of the TT PS-TIM. This balanced approach, incorporating the multiple facets of solar energy interaction with the system, further reinforces the precision and reliability of the proposed model in predicting complex fenestration system performance.

3. Experimental validation for numerical investigation method

3.1. Experiment setup for validating the optical model in Ray-tracing technique

To verify the reliability of the TT PS-TIM Ray-tracing model, an advanced experimental validation was conducted. The angular intensity distribution of the light transmitted through TT PS-TIM was measured and compared with Ray-tracing simulation results. In the experiment, a 3A solar simulator 94063A from NEWPORT was employed to simulate solar radiation at an irradiance of 1000 W/m^2. The diffused Thermotropic (TT) PS-TIM prototype was mounted on a rotatable platform to adjust the solar incidence angle, and the angular output irradiance was measured using a CC-3-UV-S cosine corrector connected to an optic fiber and detected by a USB 2000 + VIS-NIR-ES spectrometer. The experimental setup is illustrated in Fig. 6.

To validate the simulation model, the angular distribution of transmitted light through the TT PS-TIM prototype was measured at different incidence angles as illustrated in Fig. 7. Specifically, measurements were taken at thirteen altitude angles ranging from −60° to 60° with an interval of 10°, and at three azimuth angles of 0°, 30°, and 60°. The TT PS-TIM prototype was placed in the path of the simulated solar radiation, and the transmitted light was detected by a CC-3-UV-S cosine corrector via an optic fiber connected to a USB 2000 + VIS-NIR-ES spectrometer.

As shown in Fig. 8, in the ray-tracing simulation, the same geometry model of TT PS-TIM prototype was developed. A surface light source with a size of 120 mm by 120 mm and the same irradiance intensity as the solar simulator was used.

3.2. Experiment setup for thermal model validation in CFD

For thermal numerical model validation, the TT PS-TIM prototype was placed within a black chamber box and exposed to 1000 W/m^2 irradiation from the NEWPORT 3A solar simulator 94063A (shown in Fig. 9). The chamber stored heat from the solar simulator to create a discernible air temperature difference on each side of the prototype. The prototype and chamber were mounted on a rotatable platform to adjust the solar incidence angle. A fan outside the prototype prevented overheating and maintained a steady forced air flow, facilitating later convection heat transfer coefficient calculations. T-type thermocouples were used to measure the temperature of the surface, external/internal air, and slat interval air, with data recorded using a DT-85 data taker connected to a computer. The thermal image camera was also used for the surface temperature measurement to ensure the accuracy. As shown in Fig. 10, there are five thermocouples on each side surface, and three thermocouples measure the slat interval air temperature. Testo 405-V1 mini-Anemometer was used for air speed measurement. In CFD simulation, a two-dimensional model with the same size and structure as the test protype was developed for comparison.

The convection types on each side of the model are different as outside is forced convection and inside is natural convection. Thus, the

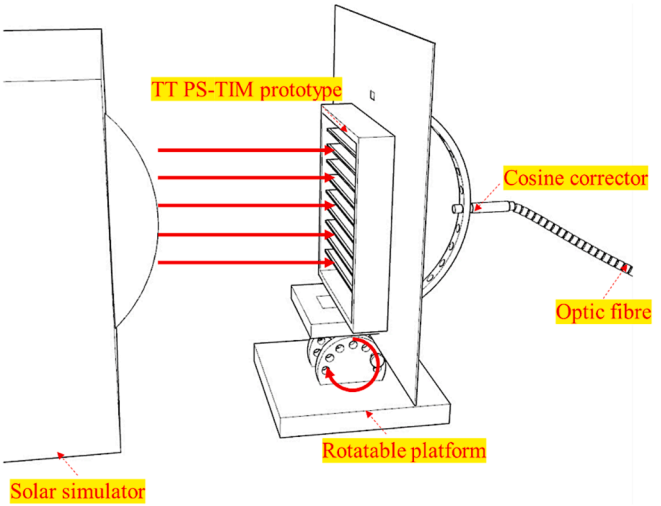

Fig. 6. Experiment apparatus for Ray-tracing simulation validation.

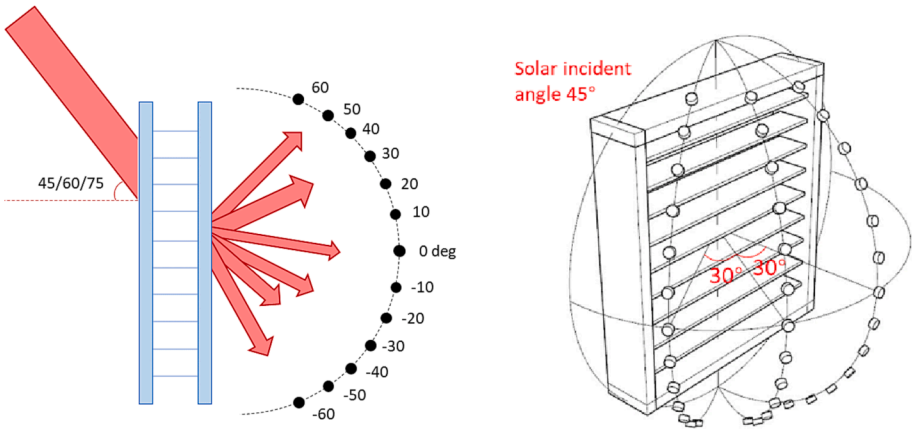

Fig. 7. Schematic diagram of the irradiance distribution measurement.

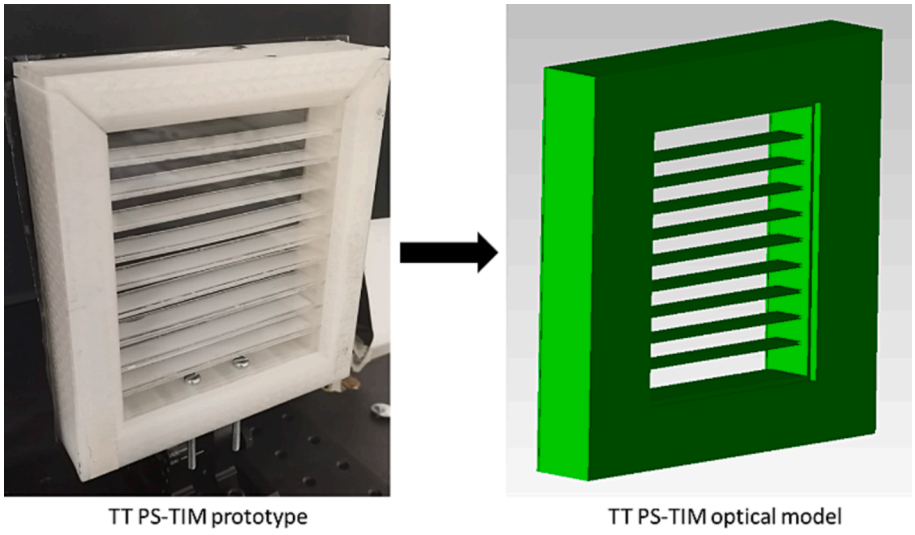

Fig. 8. Numerical model in ray-tracing technique.

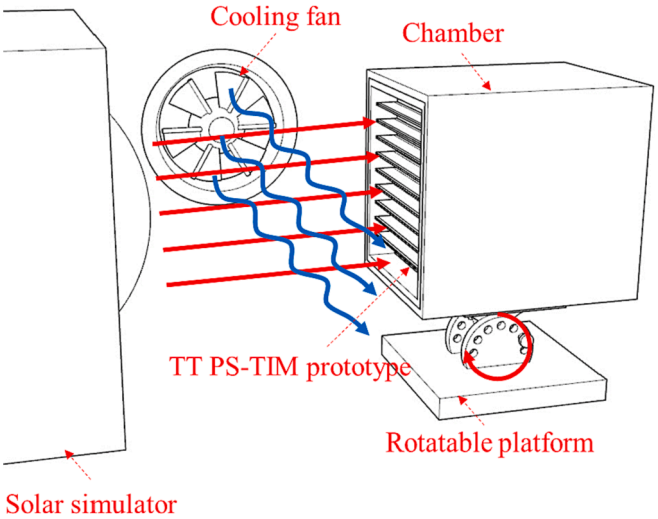

Fig. 9. Experiment apparatus for CFD simulation validation.

Nusselt number in **Equation 2** was used to calculate the plane forced convection heat transfer coefficient.

$$Nu = \frac{hL}{k} \tag{2}$$

Where h is the convective heat transfer coefficient of the flow (W/m^2·K), L is the characteristic length (m), and k is the thermal conductivity of the fluid (W/m·K). In this study, the characteristic length of external flow on flat plate equals to the distance from the leading edge.

The general equation of Nusselt number for forced convection is $Nu = f(Re, Pr)$. For natural convection, it is $Nu = f(Gr, Pr)$. The Reynolds number can be determined by the following equation:

$$Re = \frac{\rho u L}{\mu} \tag{3}$$

Where ρ is the density of the fluid, kg/m^3.

u is the flow speed, m/s.

μ is the dynamic viscosity of the fluid, kg/m·s.

The critical Reynolds number is associated with the laminar-turbulent flow transition. for flow over a flat plate, the generally accept value of the critical Re is Re = 500000. In this experiment, the highest local Reynolds number of external flow is lower than critical value. Thus, the external flow can be assumed as laminar.

For the forced external laminar flow, the Nusselt number can be also obtained by Reynolds number and Prandtl number:

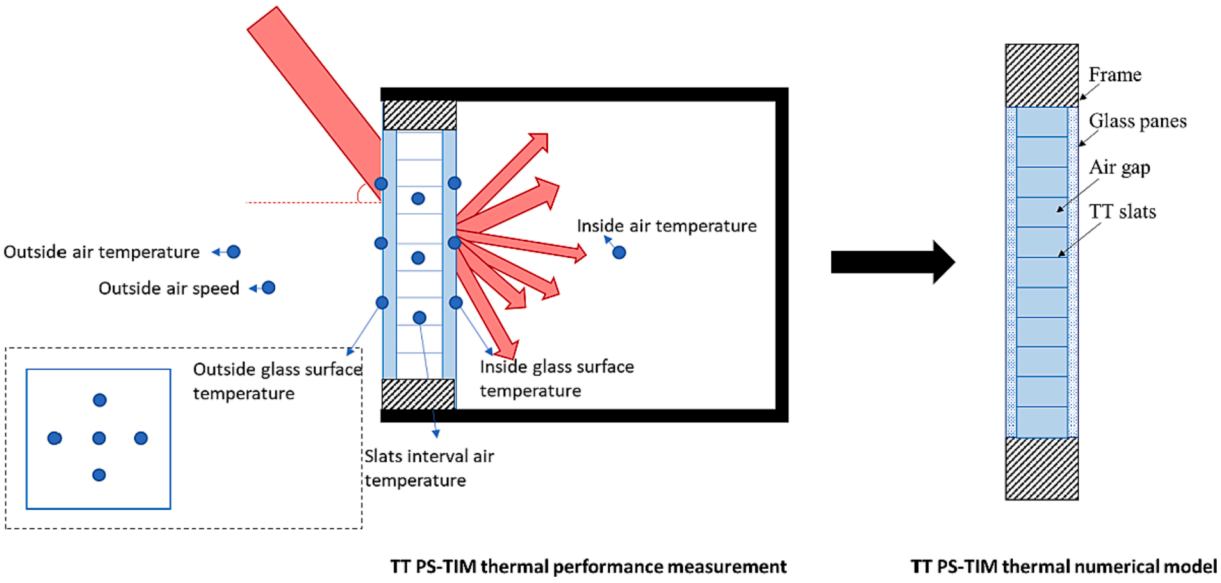

Fig. 10. Experimental measurement and numerical model development.

$$Nu = 0.332Re^{1/2}Pr^{1/3} \quad (4)$$

For inside vertical natural convection, the Nusselt number can be calculated based on the Grashof number and Prandtl number:

$$Nu = 0.59Gr^{1/4}Pr^{1/4} \quad (5)$$

where the Grashof number can be calculated by the following equation:

$$Gr = \frac{g\beta(T_{si} - T_{ai})L^3}{\nu^2} \quad (6)$$

Where, g is gravitational acceleration due to earth.

β is the coefficient of thermal expansion (equal to approximately 1/T for ideal gases), 1/K.

T_{si} is the surface temperature, K.

T_{ai} is the bulk temperature, K.

L is the vertical length, m.

ν is the kinematic viscosity, m^2/s.

The density, dynamic viscosity and Pr can be obtained according to the outside/inside air temperature.

The material properties can be found in Table 1 and boundary conditions in CFD are illustrated in Table 4. The secondary heat gain (heat generation in boundary conditions) was conducted by using Ray-tracing simulation based on the solar incidence and irradiance intensity.

3.3. Validation results

Fig. 11 displays the numerical and experimental findings on the distribution of irradiance intensities for the TT PS-TIM subjected to a 45° solar incident angle at thirteen altitude angles, spanning from −60° to 60° at 10-degree intervals, under azimuth angles of 0°, 30°, and 60°. As depicted in Fig. 11(a), the irradiance distribution within the upper region of TT PS-TIM's outgoing hemisphere is non-uniform, attributable to the specular reflection from the PMMA slices. Fig. 11(b) demonstrates the congruence between the measured and simulated outcomes at varying output angles. It is evident that the detected light intensity attains its maximum at approximately a 50° output angle when the azimuth angle is 0°, 30°, or 60°. A noteworthy concordance is observed between the simulation and experimental results.

Fig. 12 presents the numerical and experimental data on the irradiance intensity distribution of the TT PS-TIM when subjected to solar incident angles of 45°, 60°, and 75° at thirteen altitude angles, ranging from −60° to 60° with 10-degree intervals, under a 0° azimuth angle. The results indicate that at a 45° solar incident angle, the detected light intensity achieves its peak value of approximately 60 W/m^2 at a 50° output angle. This value decreases to 26 W/m^2 at a 40° output angle when the solar incident angle is 60° and further diminishes to around 10 W/m^2 at a −40° output angle under a 75° solar incidence. Overall, a strong correspondence between the simulation and experimental findings is observed. However, some discrepancies between the numerical and experimental results are noted. These differences may arise from factors such as the sealing glue, spacers within the TT slats, and shape deformation of the PMMA slices caused by stress from the weight of the TT hydrogel, which may alter the light directions and were not accounted for in the optical model.

Fig. 13 presents the numerical and experimental results of the slat interval air temperature for the TT PS-TIM. It is evident that the slat interval air temperature of the model is highest under a 45° solar incident angle and lowest with a 15° solar incidence. The average surface temperature results, illustrated in Fig. 14 **(a)**, follow the same pattern as Fig. 13 (a). In terms of error analysis, as illustrated in Fig. 13 (b) and 14 (b), the absolute difference between the simulation and experimental results is less than 1 °C and the difference in percentage in lower than 5 %, indicating a high level of accuracy and reliability in the simulation. This small discrepancy can be attributed to factors such as the TT slats shape change or light diffusion by the slat sealing glue. Despite these factors, the close alignment between the simulation and experimental results validates the effectiveness and precision of the simulation for further numerical investigations.

Table 4
CFD boundary conditions for experimental validation.

	Scenario 1	Scenario 2	Scenario 3
Inside air temperature (K)	303.0 (29.8 °C)	306.7 (33.5 °C)	306.3 (33.1 °C)
Outside air temperature (K)	302.0 (28.8 °C)	300.4 (27.3 °C)	299.2 (26.1 °C)
Solar radiance on window surface (W/m^2)	500	500	500
Solar incidence (°)	15	30	45
Slat Hear generation rate (W/m^3)	62,430	112,414	136,034

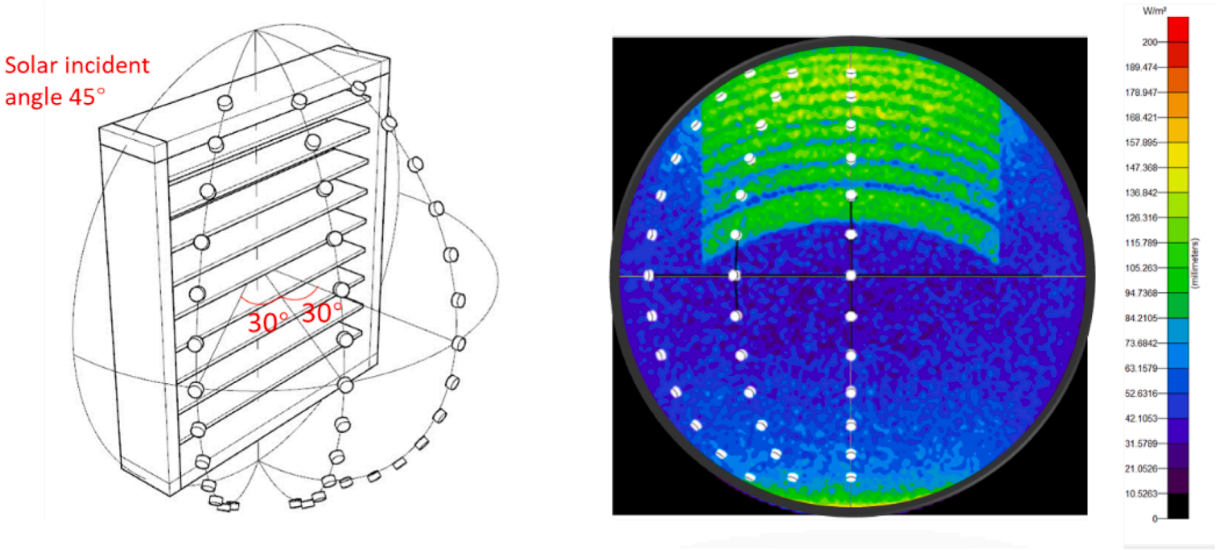

(a)

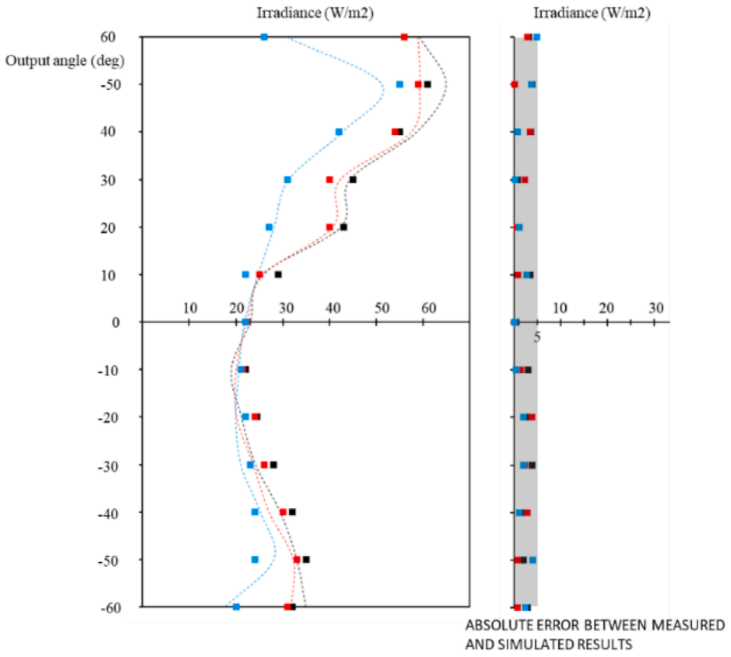

(b)

Fig. 11. The outgoing hemisphere irradiance distribution (a) and measured/simulated output angular irradiance distribution (b) of TT PS-TIM under 45° solar incident angle.

4. Results and discussion

4.1. Ray-tracing results of TT PS-TIM affected by different TT slats interval and hydrogel concentrations

Fig. 15 illustrates the overall transmittance of TT PS-TIM with different TT slats intervals in both clear (Fig. 15 **(a)**) and translucent (Fig. 15 **(b)**) states under various solar incident angles. It can be seen that for all the cases, with the increase of incident angle, there is a significant decrease of overall transmittance. This is mainly because of the reflection of the external glass pane and the internal slat absorption. In terms of the TT slat interval effect, when it is in the clear state (Fig. 15 **(a)**), the system possessing larger TT slat intervals can provide higher solar radiation transmission due to less internal reflection and solar absorption from the slats. However, the difference after the modulation of TT slat intervals is not significant, because of the low solar absorption of the clear slats. For example, the overall transmittance under 60° solar incidence reduces from 0.42 to 0.33 when the TT slats interval decreases from 10 mm to 3 mm. When the system transitions from clear state to translucent state (Fig. 15**(b)**), the TT PS-TIM window under scenarios with solar incidence between 10° and 80° experiences a significant reduction in transmittance (up to 0.5 transmittance reduction).

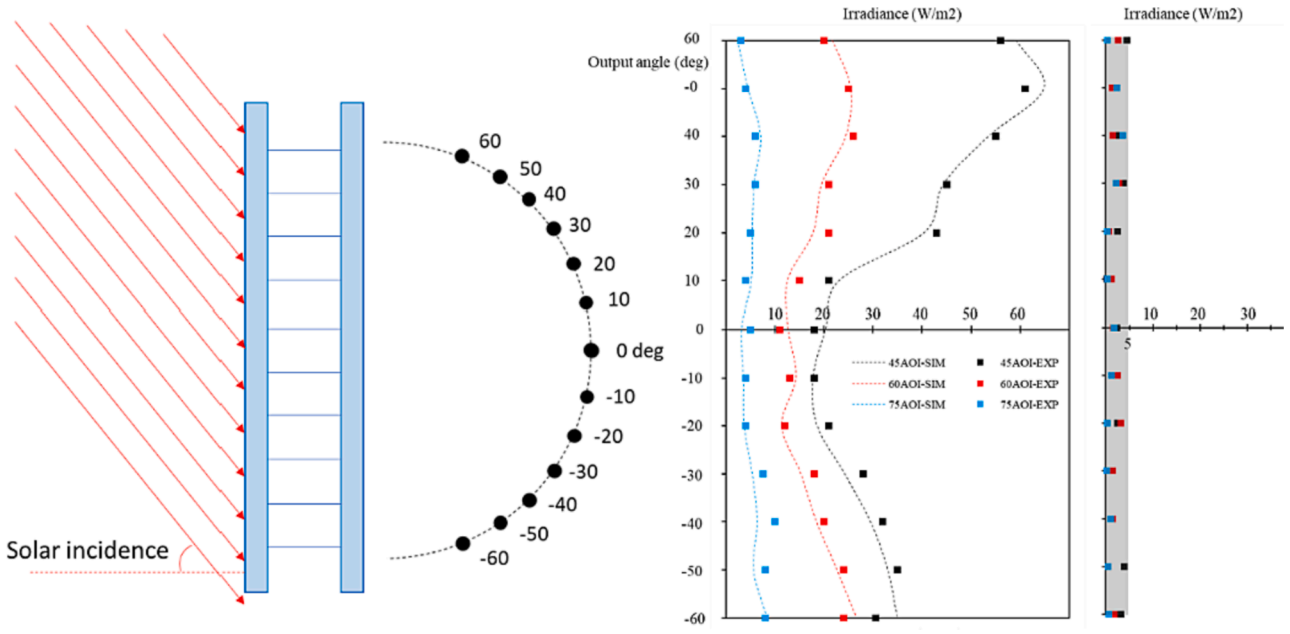

Fig. 12. The measured/simulated output angular irradiance distribution of TT PS-TIM under solar incident angles of 45°, 60° and 75°.

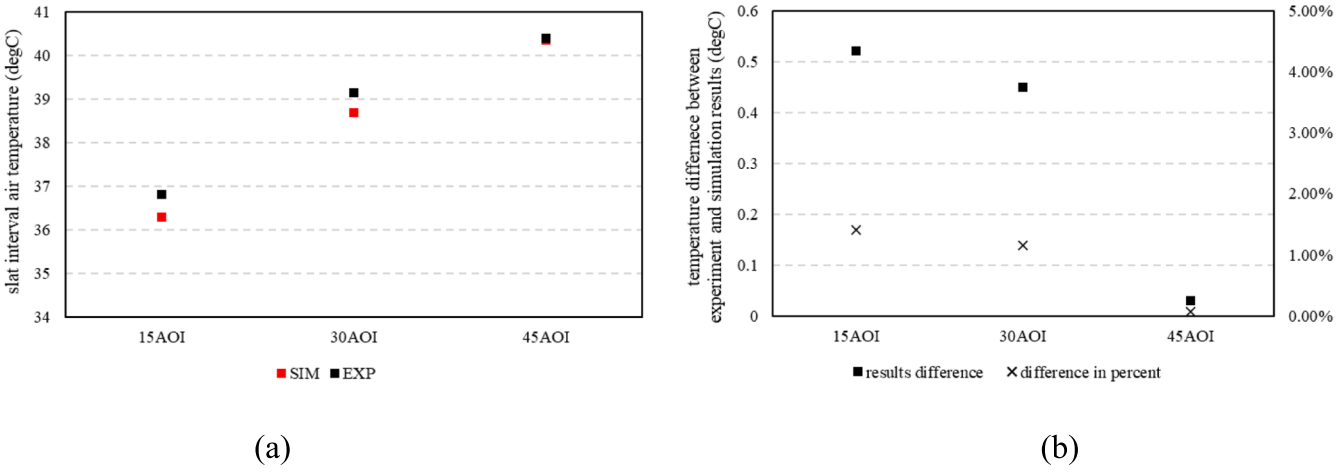

Fig. 13. The measured and simulated slat interval air temperature (a) and the difference between two methods (b).

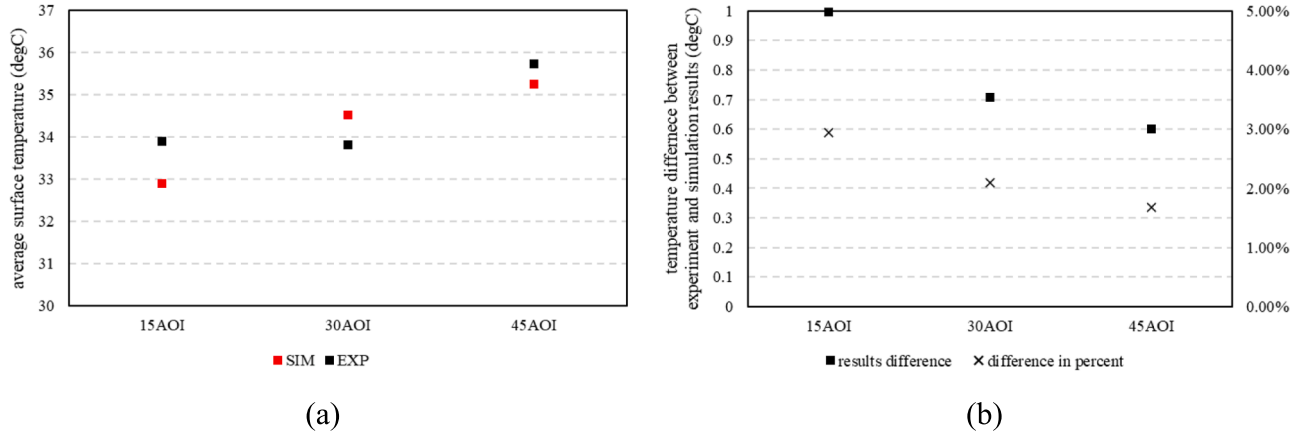

Fig. 14. The measured and simulated outside surface temperature (a) and the difference between two methods (b).

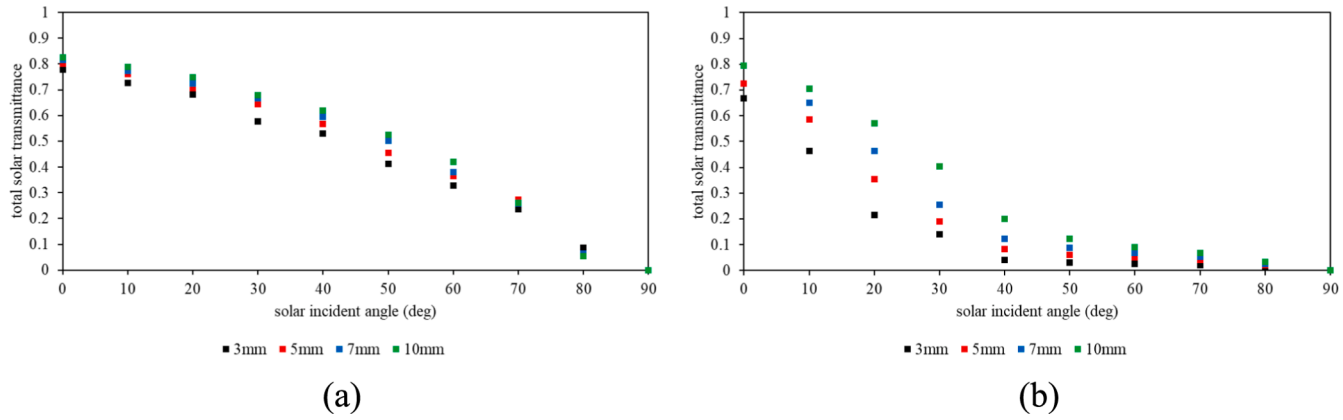

Fig. 15. Total solar transmittance of TT PS-TIM under clear (a) and translucent (b) state with different slat intervals.

Moreover, the transmittance of the model, when subjected to a 0° solar incident angle, undergoes a minor decrease in the translucent state, primarily attributed to the limited surface area of the slats exposed to solar radiation. This signifies less directly transmitted solar radiation is allowed through the system in the translucent state when compared with its clear state because of increased light attenuation (including light scattering and absorption). Moreover, the transmittance of the system decreases significantly when the interval between translucent slats is decreased from 10 mm to 3 mm (for instance, about 0.5 transmittance reduction can be found under 30° solar incidence when slat interval decreases from 10 mm to 3 mm). It is because small slats interval under translucent state has significant reduction of slat solar absorption in comparison with system possessing larger slat intervals.

Fig. 16 shows the influence of the TT slats interval on each slat solar absorption per area (W/m^2) of TT PS-TIM window in both clear (Fig. 16 **(a)**) and translucent state (Fig. 16 **(b)**). In the clear state, the TT slats solar absorption reaches the highest at 60° compared with other solar incidence angles. This is because 60° solar incident light rays cause more internal reflection, interaction and being absorbed more times with slats. The interval between TT slats exerts a relatively insubstantial effect on the solar absorption of each slat in clear state. This indicates that, as the solar incident angle increases, systems with smaller slat intervals demonstrate a heightened capacity for absorbing solar energy, attributable to their increased number of slats. When it transitions to translucent state (Fig. 16 **(b)**) from clear state, attributed to the increased reflection and scattering of light rays within the structure, the absorption of TT slats increases significantly. The solar absorption per slat in models subjected to solar incident angles between 10° and 80° significantly surpasses that of the model under a 0° and 90° solar incidence. This is attributable to the fact that the slats in model under 0° solar incidence have restricted surface area exposed to solar radiation, causing most light rays to penetrate the dual glass panes without undergoing slat-mediated scattering or absorption. When the solar incident angle is close to 90°, the reflection of the front glass blocks most of the solar incidence. Due to variations in the areas exposed to solar incident light rays, the slat unit of the system with a 3 mm slat interval records the highest solar absorption at an almost 0° solar incident angle. On the other hand, slat units in systems with 5 mm, 7 mm and 10 mm slat intervals record their maximum absorption rates under solar incidences of 20°, 30°, and over 40° respectively. The results provide invaluable insights into light absorption under varied circumstances, thereby facilitating more accurate computations of indoor indirect solar heat gain in computational fluid dynamics (CFD) simulations.

4.2. *Solar heat gain coefficient investigation for TT PS-TIM*

Fig. 17 illustrates the Solar Heat Gain Coefficient (SHGC) for TT PS-TIM under both clear and translucent slate, with variations according to solar incident angles. This diagram draws upon Equation 1 outlined in **Section 2.2.2**, and bears similarity to the rule of transmission highlighted in Fig. 15. As the solar incidence increases, the SHGC of TT PS-TIM exhibits a decrease, attributable to the reflection occurring on the outer glass surface. In the clear state, as shown in Fig. 17**(a)**, a system with greater TT slat intervals results in a higher SHGC. This phenomenon can be explained by a reduced level of internal reflection and solar absorption from the slats. However, the SHGC of the overall system isn't significantly affected by the modulation of TT slat intervals, as a result of the clear slats' low absorption and high transmission. A remarkable shift

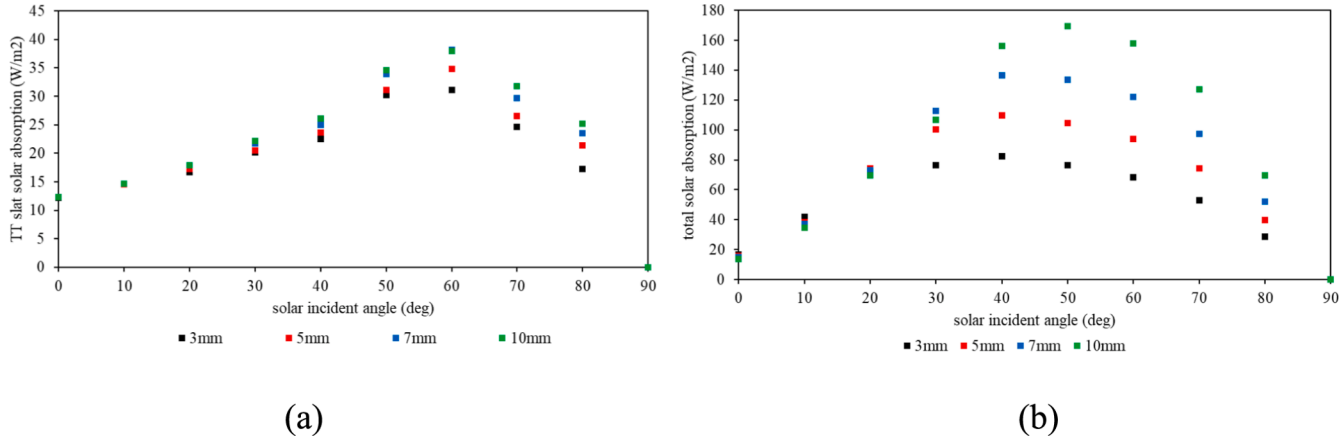

Fig. 16. Solar absorption of TT slat in TT PS-TIM under clear (a) and translucent (b) state with different slat intervals.

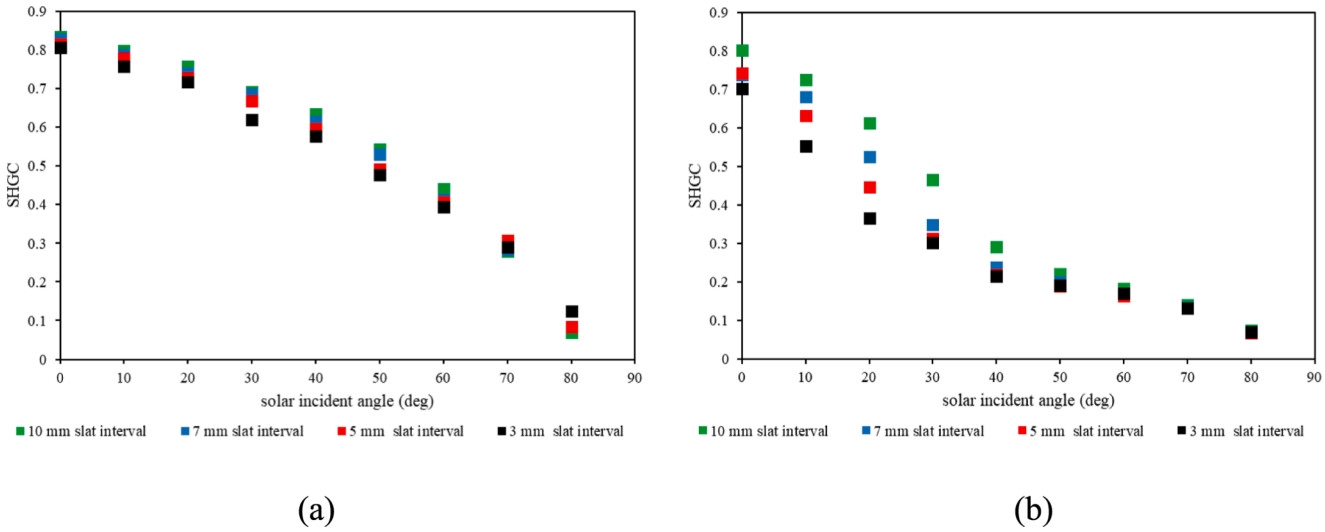

Fig. 17. Solar heat gain coefficient (SHGC) of TT PS-TIM in clear state (a) and translucent state (b) under different solar incidence.

occurs when the system transitions from a clear state to a translucent state, as depicted in Fig. 17**(b)**. In scenarios where solar incidence ranges from 20° to 70°, there is a notable reduction in SHGC values observed in the TT PS-TIM window. However, the variation in SHGC values is relatively insignificant when the solar incidence is in close proximity to 0° and 90°. That is because at solar incidence near 0°, the area exposed to solar radiation is relatively restricted, which results in minimal heat gain difference among all scenarios. Conversely, when the solar incidence approaches 90°, the majority of the solar radiation is obstructed by the reflective properties of the front glass, thus blocks most of the solar incidence and results in low SHGC in all models. It's important to note that the influence of slat intervals on the SHGC of TT PS-TIM under the translucent state becomes more pronounced when the solar incident angle is less than 50°. This can be attributed to the outer glass reflection impeding most of the solar energy from the external environment at larger solar incident angles. Owing to the secondary heat gain from the absorbed solar energy within the TT slat, the discrepancy across these scenarios is smaller when compared to the transmission results found in Fig. 15**(b)**. For instance, when the solar incidence is at 20°, a reduction in slat interval from 10 mm to 3 mm leads to a decrease in the SHGC of TT PS-TIM from 0.61 to 0.36. However, this trend differs from the transmission results (Fig. 15) where the same slat interval change results in a decrease from 0.57 to 0.21. This emphasizes the distinct impact that different slat intervals can have on the SHGC of TT PS-TIM, particularly under different states and solar incidence angles.

4.3. Numerical investigation of TT PS-TIM transition point

Fig. 18 illustrates the simulated temperature contours for the window systems under different TT slat intervals (3 mm, 5 mm, 7 mm, 10 mm) with and without solar radiation. A solar incidence angle of 30° serves as the representative example for this analysis, with the slats in both clear and translucent states. When there is no solar radiation (Fig. 18 **(a)**), the internal air temperature distribution is solely affected by convection which is driven by the temperature difference between the two glazing panes. When solar radiation of 500 W/m^2 radiates on the clear slats (Fig. 18 **(b)**), a portion of solar energy is absorbed by the TT slats and the slat temperature increases compare with that in no solar radiation condition. Notably, the slat temperature exhibits a higher value in the system with a smaller slat interval. For instance, the slat temperature of the TT PS-TIM with a 3 mm slat interval is approximately 36 °C, the value that diminishes to roughly 31 °C when the slat interval expands to 10 mm. When the slats are in translucent state (Fig. 18 **(c)**), the absorption and subsequent release of solar energy by the TT slats increase significantly, leading to a considerable rise in slat temperature. Among all the models, the system with a 3 mm slats interval exhibits the highest slat temperature of 44 °C, while the one with a 10 mm slat interval records a slat temperature of approximately 40 °C. The results indicates that the solar absorption and release can help to increase the temperatures of the TT slats so that they can transit into translucent state more easily, especially for those with smaller slat intervals.

Fig. 19 illustrates the critical average surface temperature of the outdoor/indoor glasses for the TT PS-TIM transiting from clear to translucent state under different solar absorption of the TT slat unit. It can be conducted that as the solar absorption by each TT slat in TT PS-TIM escalates, the critical average surface temperature of the glasses required for the TT PS-TIM transition diminishes. This reduction in the critical temperature accelerates with increased slat intervals. For instance, when the TT slat interval is configured to 10 mm, the critical average surface temperature of the glasses exhibits a 0.3 °C reduction as each slat's solar absorption surges from 0 to 60 W/m^2. However, this decrease becomes more prominent with smaller slat intervals, rising to 0.5 °C and 1.3 °C when the slat intervals are 7 mm and 5 mm respectively. The reduction reaches its highest value of 4.9 °C with the smallest slat interval at 3 mm. These results provide compelling evidence that the solar absorption of the TT slat significantly impacts the transition process of TT PS-TIM under a dynamic outdoor environment. These key insights are instrumental in guiding the predictive analysis of thermal performance, particularly during the transition from transparent to translucent states in the TT PS-TIM system. Thus, it becomes essential to incorporate factors such as solar absorption rates of TT slats and their intervals when modelling or predicting the system's thermal behaviour in further numerical annual energy or daylight performance investigation.

4.4. Thermal performance of the TT PS-TIM in summer and winter days

The findings elucidated in **Section 4.3** indicate that the transition point of the TT PS-TIM is influenced by a combination of factors, namely the surface temperature of the indoor/outdoor glasses, the solar energy absorption capacity of the TT slat, and the slat interval within the TT PS-TIM. To have an in-depth comprehension of the thermal performance of TT PS-TIM, transient Computational Fluid Dynamics (CFD) models of TT PS-TIM, incorporating various slat intervals, have been constructed and assessed under both summer and winter weather conditions prevalent in London. These models have factored in a transition temperature of the TT slat set at 32 °C, indoor air temperature of 26 °C in summer and 21 °C in winter, as well as the heat convection coefficients of the outside and

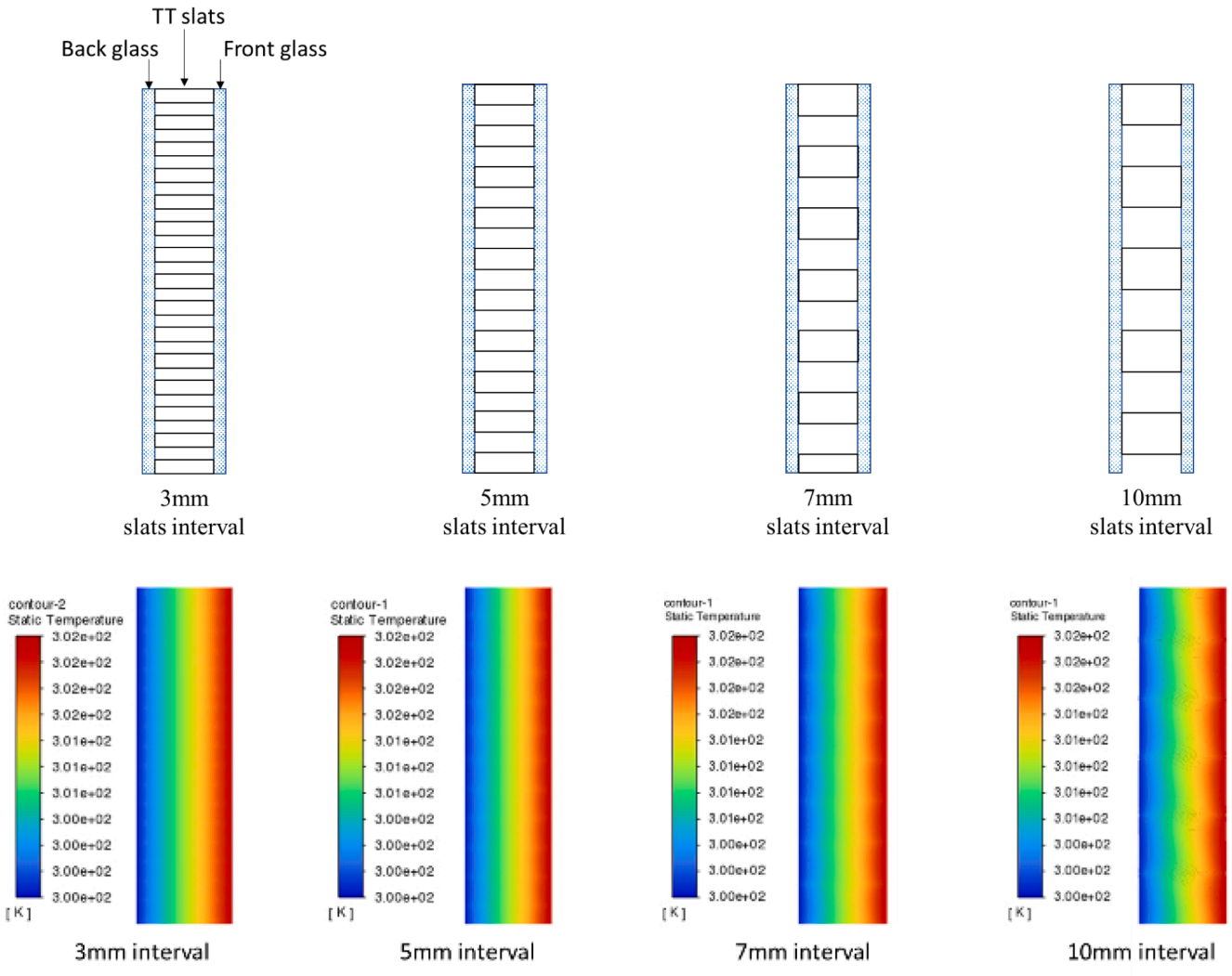

Fig. 18. Temperature contours for different conditions: (a)no solar radiation; (b)clear state; (c)translucent state and models within the fluid area.

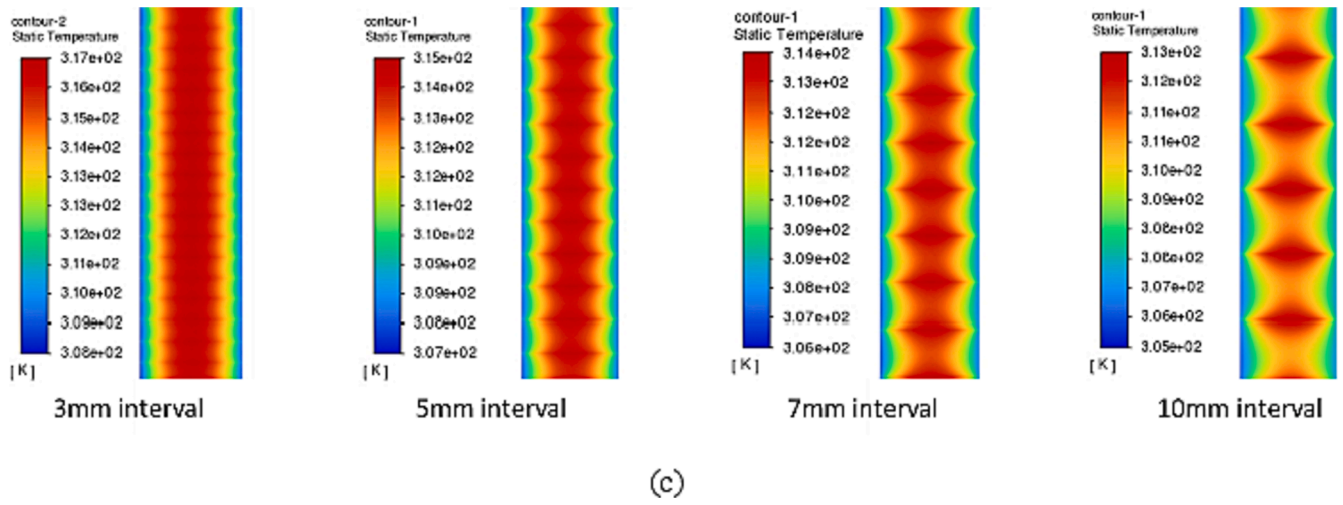

(c)

Fig. 18. (*continued*).

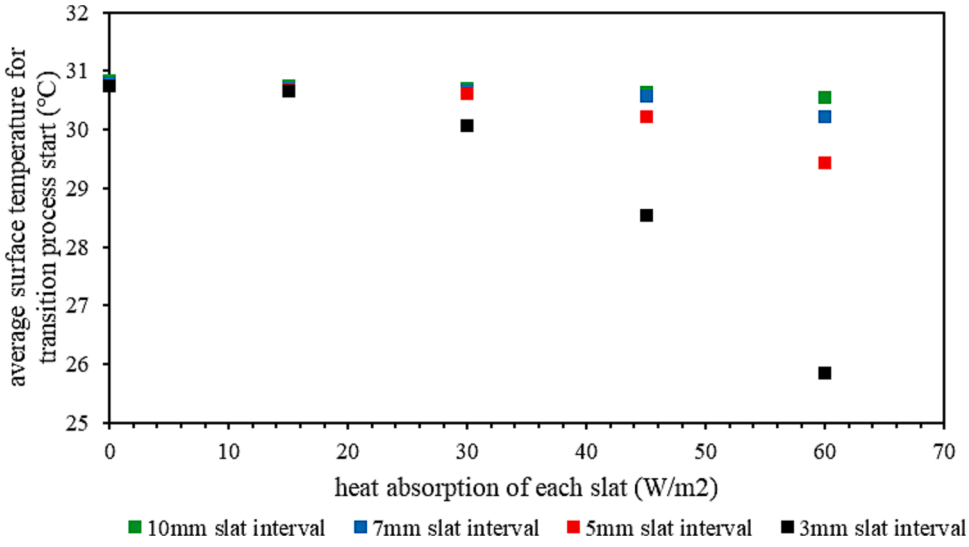

Fig. 19. The critical average surface temperature of outdoor/indoor glasses for TT PS-TIM transition affected by TT slat unit solar absorption.

inside surfaces set at 8 W/(m^2·K) and 2.5 W/(m^2·K) respectively. Fig. 20 details the weather conditions across three consecutive days that were utilized for the simulation input. These conditions includes direct solar radiation (I_{dr}), diffuse radiation (I_{ds}), ground reflection radiation (I_{dg}), and outdoor dry bulb air temperature (T_a), captured during both summer (Fig. 20(a)) and winter (Fig. 20(b)) periods in London. The data for these simulations is drawn from the annual weather files in the EnergyPlus Weather Format (EPW), offering hourly climate data derived from International Weather for Energy Calculations (IWEC) meteorological information.

To facilitate a comprehensive analysis of the thermal performance of TT PS-TIM, numerical investigations into the dynamic total heat gain and heat loss during summer and winter periods have been conducted. Fig. 21 illustrates a schematic of the heat gain/loss emanating from the TT PS-TIM system during these seasons. In summer, the total heat influx into the indoor environment can be primarily seperated into two components: the heat transferred from the window system and the transmitted solar energy. In winter, the transmitted solar energy can reduce the heat loss from window. The proportion of solar energy transmitted or absorbed is influenced significantly by two principal factors: the direct solar radiation and the indirect solar radiation, which encompasses sky diffused radiation and ground reflected solar radiation. The calculation of diffuse transmittance and absorption of the window system can be obtained by executing an integral over the angular solar light beam transmittance and absorption, drawing upon the results of Ray-tracing simulations [63].

Fig. 22 presents an analysis of hourly temperature of TT slat (Fig. 22 **(a)**), the transmitted solar energy (Fig. 22**(b)**), heat transferred from the window system (Fig. 22**(c)**), overall heat gain (Fig. 22**(d)**) experienced by the TT PS-TIM under varying slat intervals, and a comparison with traditional Double Glazing (DG) over a three-day period in summer. Furthermore, the integrated heat gain of these systems is also captured in Fig. 22**(e)**.

The results illustrate that the solar transmitted energy (Fig. 22**(b)**) of the TT PS-TIM is notably inferior to that of the DG system, attributable to the TT PS-TIM's lower solar transmittance. Among all TT PS-TIM configurations, the model incorporating a 3 mm TT slat interval demonstrates a significant reduction in transmitted solar energy during noon hours (for example, when time goes from hour 11 to 12, the transmitted solar energy of TT PS-TIM with 10 mm slat interval increases significantly from approximately 145 W/m^2 to 196 W/m^2, but the system with 3 mm slat interval decreases from about 140 W/m^2 to 59 W/m^2). The underlying reason for this trend is the elevation in TT slat temperature beyond its transition temperature (Fig. 22**(a)**), inducing a shift to a

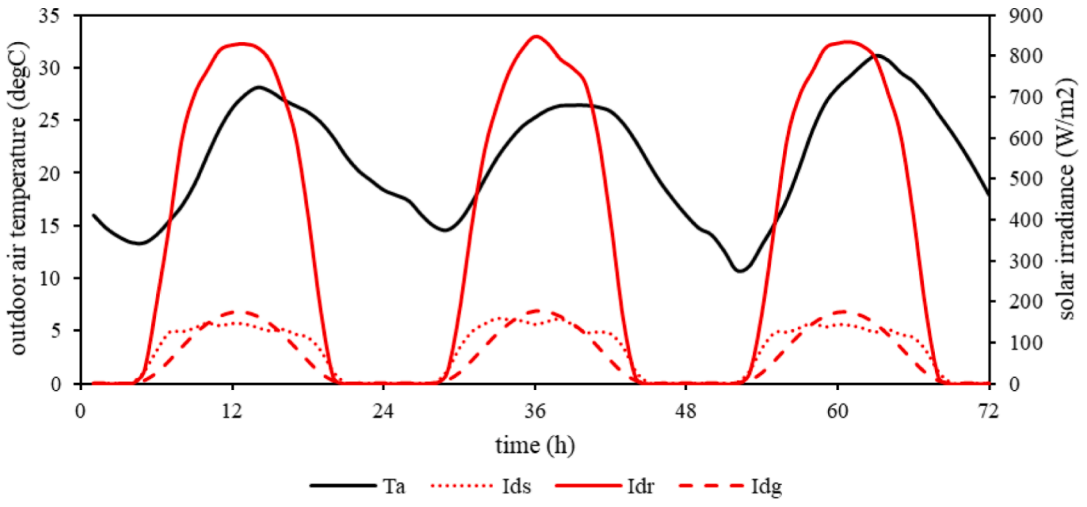

(a)

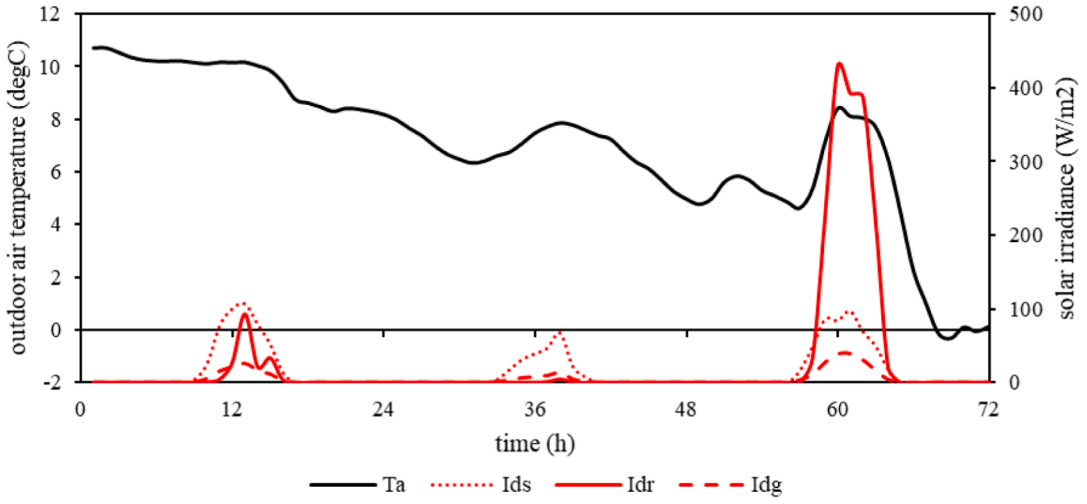

(b)

Fig. 20. Three continuous days weather conditions in summer (a) and winter (b) of london.

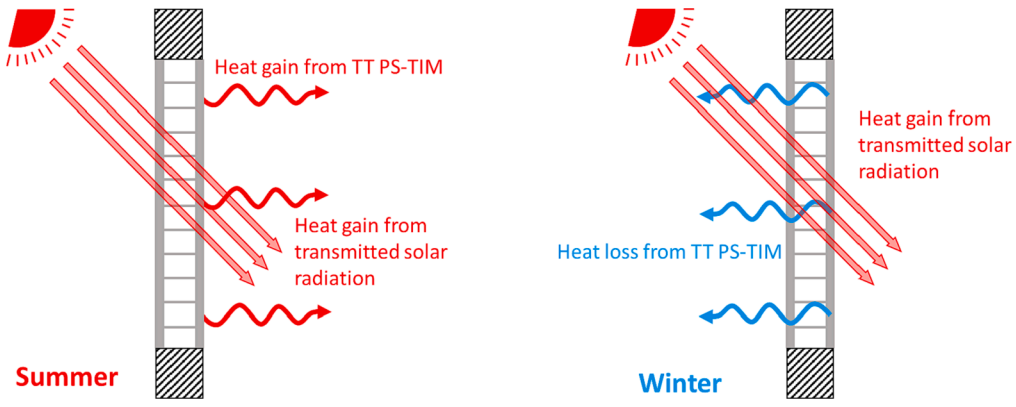

Fig. 21. Diagram of heat gain and loss from tt ps-tim in summer and winter.

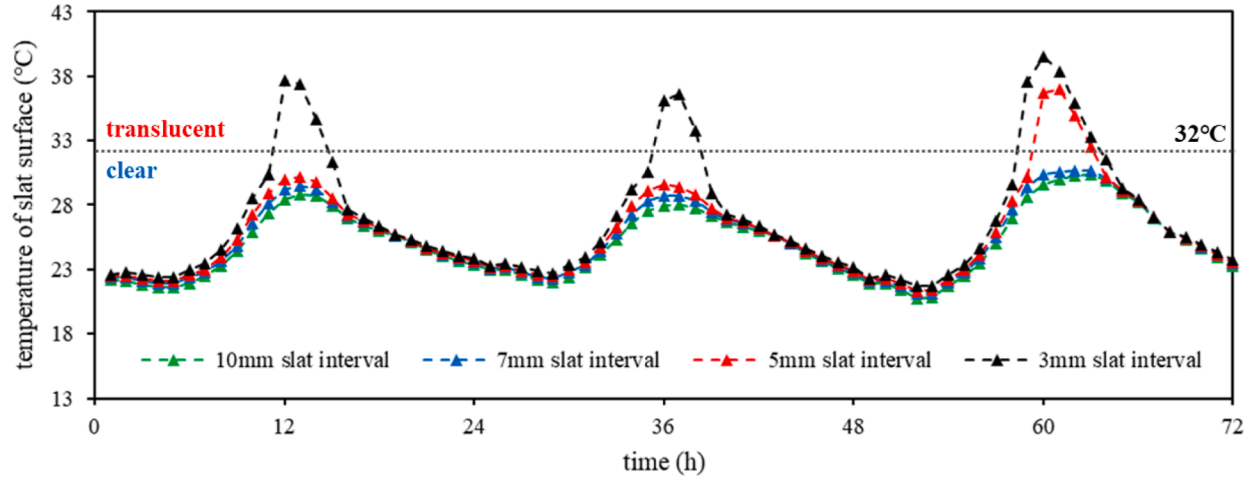

(a)

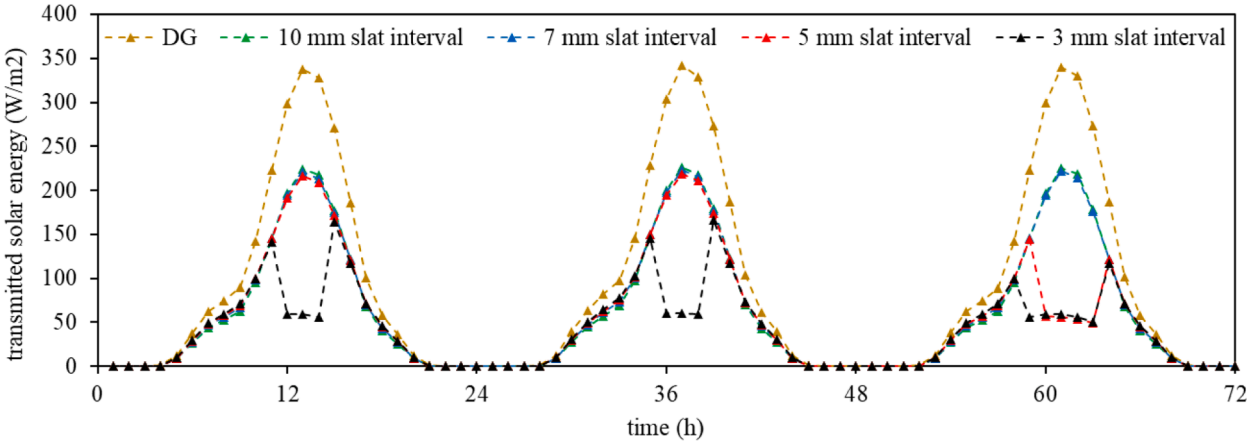

(b)

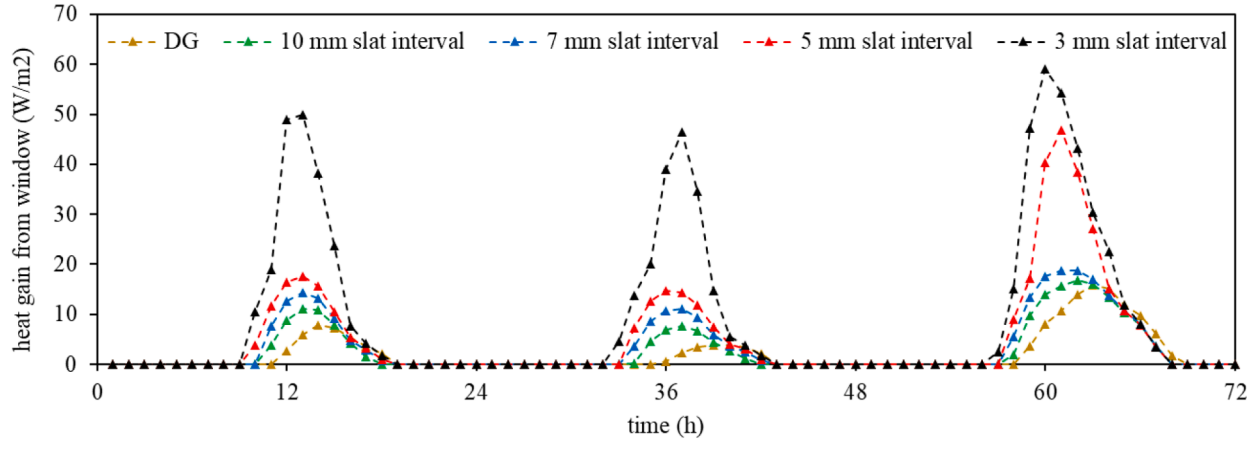

(c)

Fig. 22. (a) The surface temperature of TT slats, (b) the transmitted solar energy, (c) the heat transfer from window system and (d) the overall heat gain by the TT PS-TIM under various slat intervals and traditional Double Glazing (DG) within three continuous days in summer, and (e) the integrated heat gain of these systems.

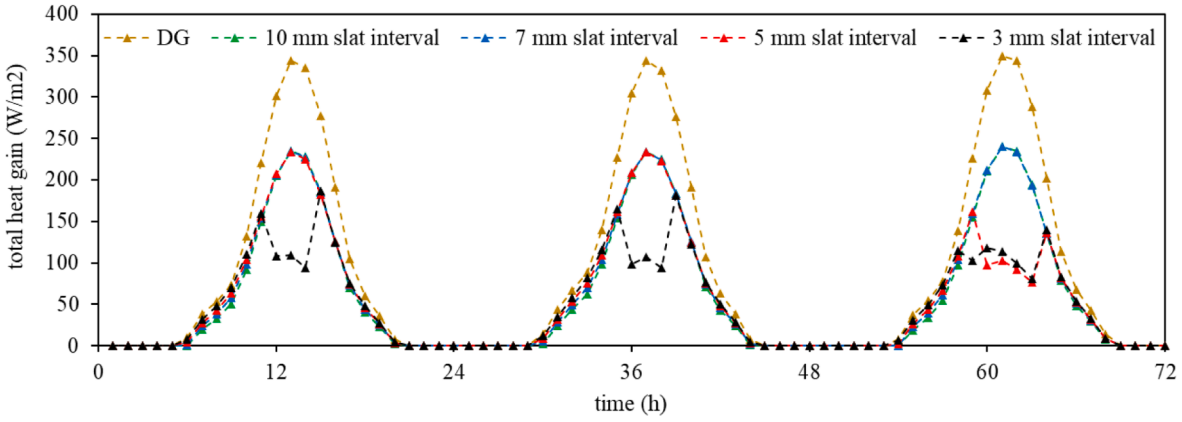

(d)

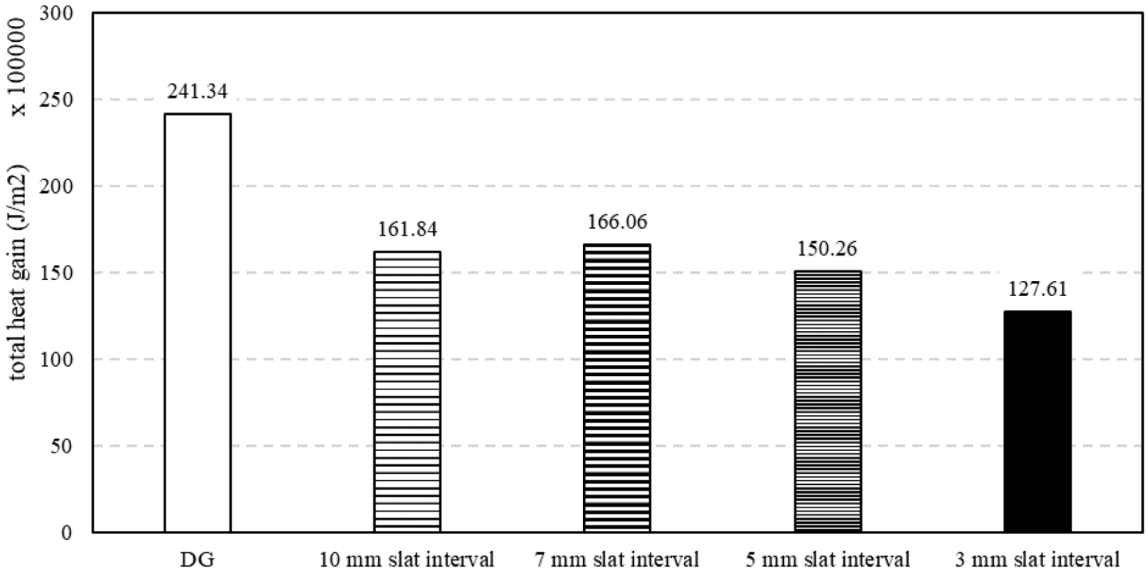

(e)

Fig. 22. (*continued*).

translucent state and thus reducing solar transmittance. Similar results are observable in the TT PS-TIM system with a 5 mm slat interval, although the transition only occurs during the noon hours of the third day, attributed to the diminished impact from slat solar absorption as depicted in Fig. 20. Furthermore, the analysis shows that the slat interval alteration does not significantly affect the transmitted solar energy of the TT PS-TIM in both clear and translucent states.

Fig. 22**(c)** illustrates that the heat transferred from the window system of TT PS-TIM is greater than that of the DG system. This can primarily be attributed to the absorption of solar radiation by the TT PS-TIM system. Furthermore, a distinct difference can be observed in the timeframe during which the TT PS-TIM and DG systems reach their peak values. This can be explained by the fact that the heat gain from the DG system is predominantly influenced by the outdoor air temperature, whereas the heat gain from the TT PS-TIM systems is more intricately determined by both solar radiation and outdoor air temperature, with a larger impact stemming from the former. Due to the clear/translucent state difference, a notable instance of this interplay is observable during the noon hours. As the day progresses from the hour 11 to the hour 12, the indoor window heat gain of TT PS-TIM with a 10 mm slat interval exhibits a marginal increase from approximately 8 W/m^2 to 11 W/m^2. Conversely, the system incorporating a 3 mm slat interval demonstrates a substantial increase, from approximately 18 W/m^2 to 48 W/m^2. This pattern is exclusive to the model with a 5 mm slat interval during the noon hours of the third day. Besides, when the TT PS-TIM is in a clear state, a system with smaller slats experiences a higher total solar absorption, which results in increased window heat gain within the indoor environment. Upon transitioning into a translucent state, models with smaller slat intervals are capable of providing a higher window heat gain.

Fig. 22**(d)** delineates the hourly overall heat gain of the different models, highlighting similar trends to those discerned in the context of transient transmitted solar energy, as displayed in Fig. 22**(b)**. This similarity is due to the substantial contribution of transmitted solar energy to the total heat gain of the window systems. Moreover, it is worth noting that the TT PS-TIM model, when in a translucent state with a 5 mm slat interval, exhibits a lower overall heat gain when compared to the model with a 3 mm slat interval. This can primarily be attributed to its lower window heat gain. Further investigation into the integrated heat gain, as demonstrated in Fig. 22**(e)**, reveals that the TT PS-TIM system markedly outperforms the traditional DG system in terms of limiting solar energy penetration into the indoor environment. For

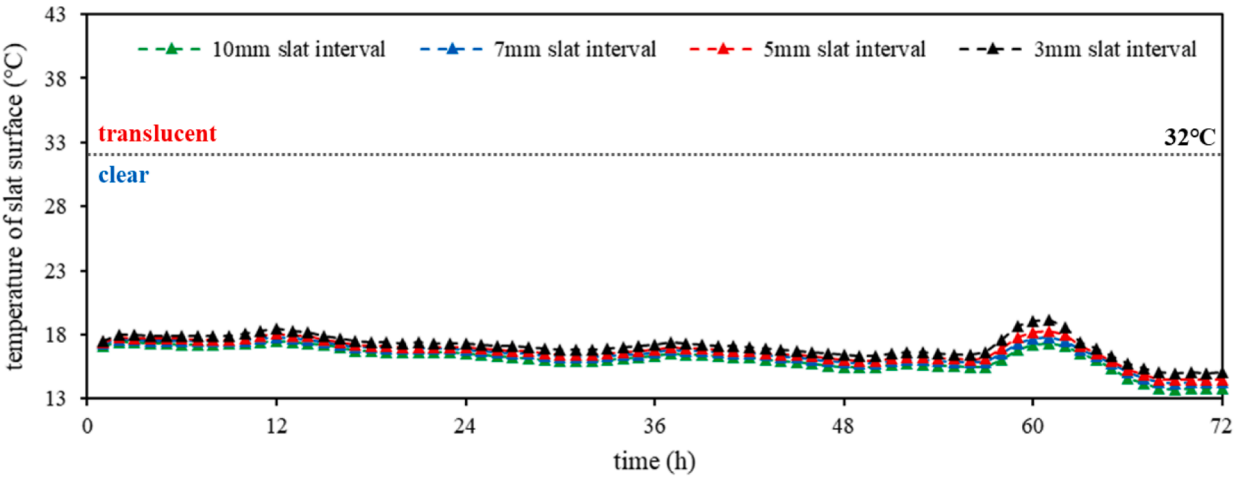

(a)

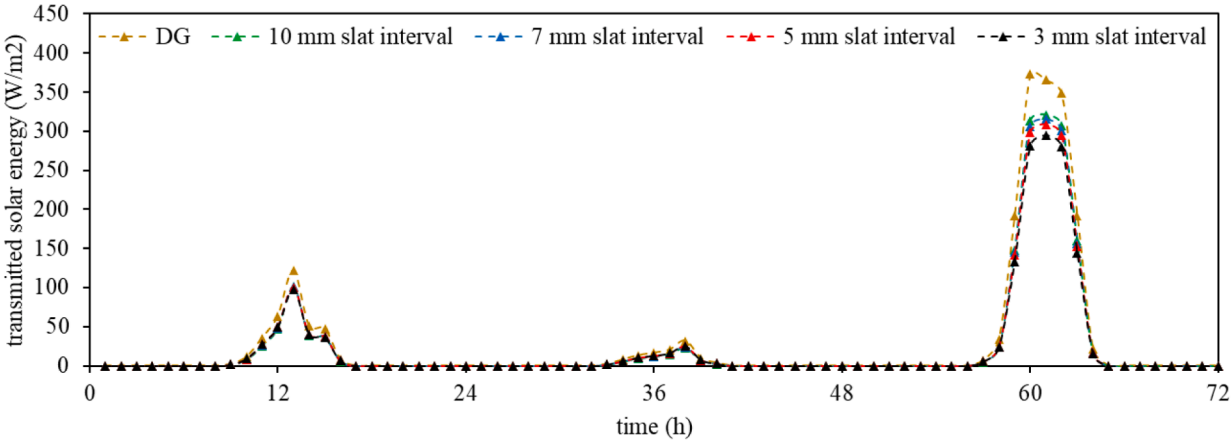

(b)

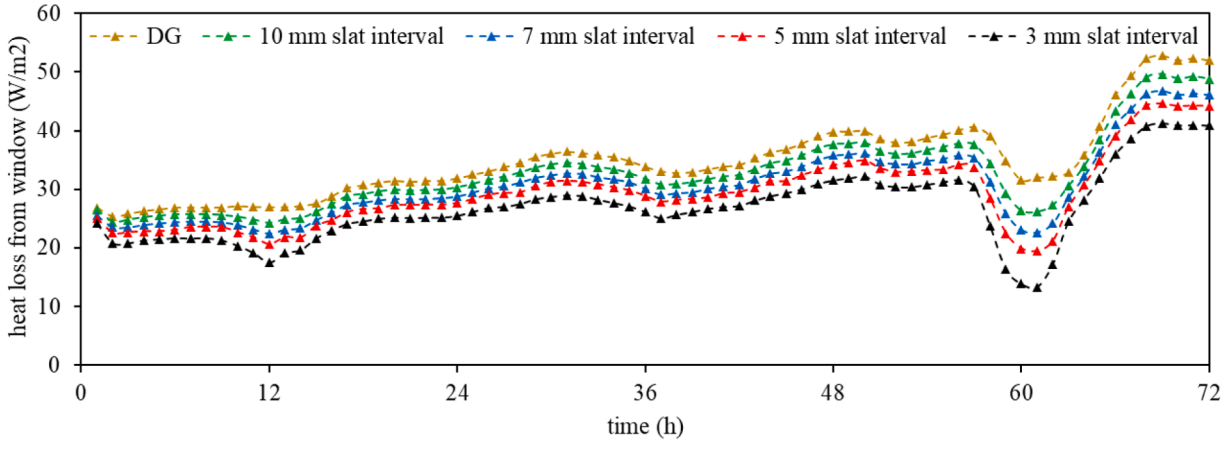

(c)

Fig. 23. The surface temperature of TT slats (a), the transmitted solar energy (b), heat transferred from window system (c) and overall heat gain (d) by the TT PS-TIM under various slat intervals and traditional Double Glazing (DG) within three continuous days in winter and the integrated heat gain (e) of these systems.

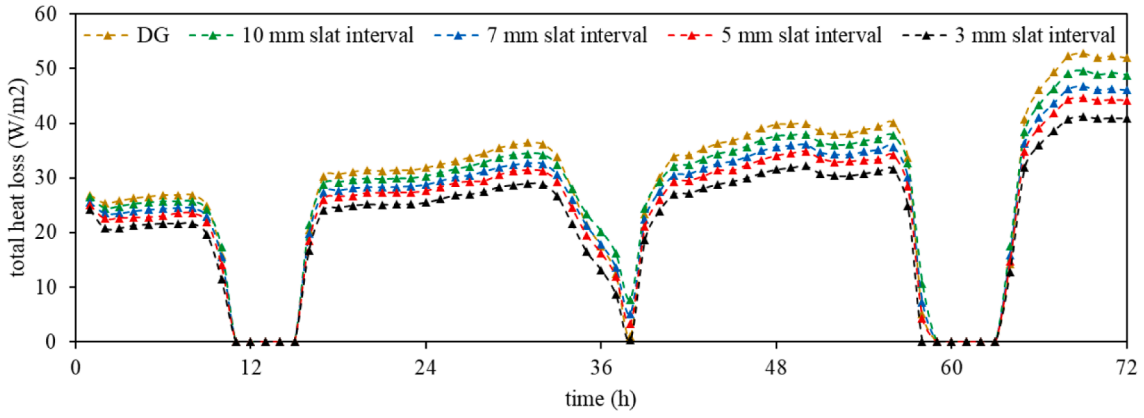

(d)

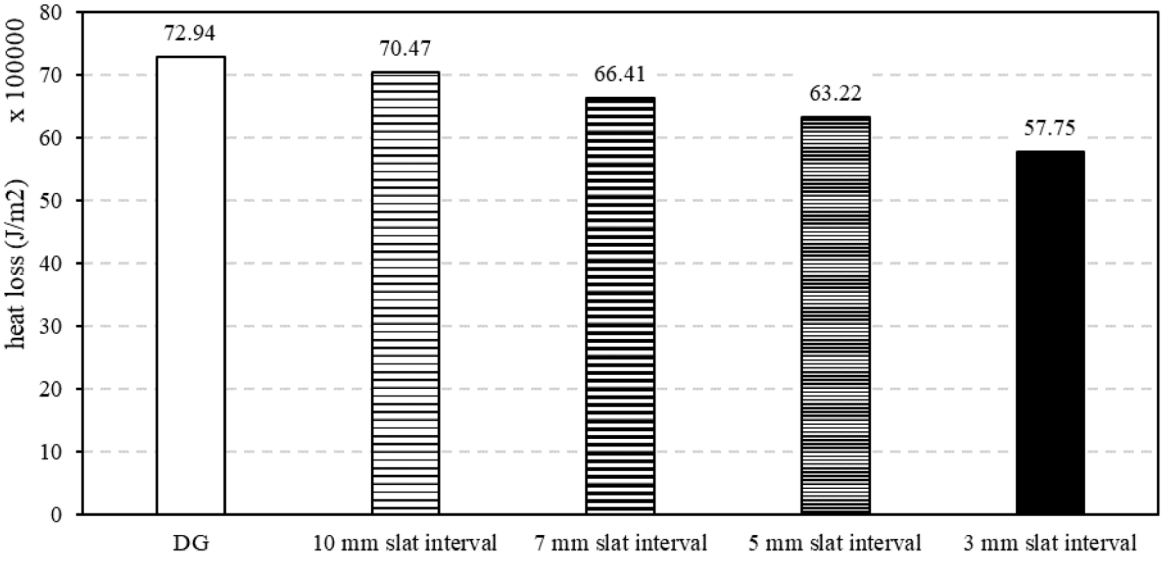

(e)

Fig. 23. (*continued*).

instance, a model of TT PS-TIM shows an integrated heat gain of 161.84 • 10^5 J/m^2, which denotes approximately a 30 % reduction when contrasted with the DG system. Among all models, the TT PS-TIM system with a 3 mm slat interval registers the lowest integrated heat gain (127.61• 10^5 J/m^2) in all scenarios. This model, due to its smaller slat intervals, spends more time in a translucent state, consequently facilitating a lower heat gain in the indoor environment. These findings underscore the role of slat interval and state transition in modulating the overall heat gain through window systems in summer.

Fig. 23 provides an illustration of hourly temperature of TT slat (Fig. 23**(a)**), the transmitted solar energy (Fig. 23(b)), heat gain from the window system (Fig. 23**(c)**), and overall heat gain (Fig. 23**(d)**) for TT PS-TIM models with various slat intervals, as well as traditional Double Glazing (DG), over three consecutive days in winter. The integrated heat gain of these systems is shown in Fig. 23**(e)**. As depicted in Fig. 23**(a)**, the temperature of the TT slats across all TT PS-TIM models consistently remains below the transition temperature of 32℃. This suggests that, over a three-day period, the slats maintain a clear state.

The findings also indicate that the transmitted solar energy of TT PS-TIM models is generally lower than that of the DG system, attributed to the lower solar transmittance of the TT PS-TIM models. However, the disparity between the TT PS-TIM and DG systems in terms of transmitted solar energy is narrower during the winter months. This phenomenon can be attributed to the typically lower solar incident angles encountered during winter, which assist in maintaining a high solar transmittance (Fig. 15 **(b)**) in the TT PS-TIM models. All TT PS-TIM models remain in the clear state throughout the winter due to lower external temperatures. As a result, the impact of the slat interval on the TT PS-TIM models during this season is marginal. Among the various models, it is notable that the one with the smallest TT slat interval exhibits the lowest transmitted solar energy into the indoor environment. For instance, when the TT slat interval decreases from 10 mm to 3 mm, there is approximately an 8 % reduction in transmitted solar energy.

Moreover, the window heat loss depicted in Fig. 23**(c)** demonstrates that TT PS-TIM has a reduced heat loss relative to the traditional Double Glazing (DG) system. This reduction can be attributed to the lower convection heat transfer within the interior air cavity of the TT PS-TIM. Intriguingly, the TT PS-TIM models with smaller slat intervals display a further reduction in window heat loss. This can be ascribed to the fact that models with narrower slat intervals have lower convection heat

transfer and enhanced secondary heat gain from solar absorption. The total heat gain across the various models is elucidated in Fig. 23**(d).** It can be discerned that the elevated solar transmission effectively mitigates indoor heat loss from window systems. Moreover, during periods devoid of solar radiation, TT PS-TIM can effectively curtail heat loss by reducing convection heat transfer, offering an advantage over the traditional DG system.

Upon evaluating the integrated heat loss across the various window systems, as displayed in Fig. 23**(e)**, it becomes evident that the TT PS-TIM achieves a lower integrated heat loss compared to the traditional Double Glazing (DG) system. This result is primarily attributed to the reduced convective heat transfer within the internal air cavity of the TT PS-TIM. Notably, the TT PS-TIM configuration with a 3 mm slat interval demonstrates superior performance, registering an integrated heat loss of 57.75 • 10^5 J/m^2. This value represents a reduction of 20.8 % when compared with the DG system, thereby emphasizing the potential energy-saving benefits of the TT PS-TIM system.

In conclusion, through the integration of Ray-tracing and Computational Fluid Dynamics (CFD) numerical simulation methods, it has been demonstrated that the thermal performance and switching states of TT PS-TIM can be accurately predicted. In a comparative analysis with the conventional Double Glazing (DG) system, the TT PS-TIM presented a distinct advantage, exemplified by reduced heat gain during summer and minimized heat loss throughout the winter period. Moreover, configurations with smaller TT slat intervals showcase more pronounced potential for energy-saving benefits, thereby emphasizing the efficacy of TT PS-TIM in realising energy-efficient solutions.

5. Conclusions

This paper presents the development and comprehensive thermal performance assessment of an innovative smart complex fenestration system, integrated with a realistically selected Thermotropic material-based Parallel Slats Transparent Insulation Materials (TT PS-TIM). The thermal performance was comprehensively analysed using a novel numerical simulation method, which integrates Ray-tracing and Computational Fluid Dynamics (CFD). This unique approach considers factors such as solar incidence and TT slat solar absorption, thereby providing highly accurate predictions of TT PS-TIM system thermal performance. To substantiate the reliability of the proposed method, validations were undertaken by comparing the numerical simulation results with experimental data. Based on the obtained results, the following conclusions can be drawn:

(1) The transmittance of TT PS-TIM experiences a substantial reduction when transitioning from a clear to a translucent state, indicating the high potential of translucent TT PS-TIM to block solar irradiance. Notably, while the slat interval has a minimal impact on transmittance in the clear state, a significant reduction—by up to 0.5 in transmittance—is observed as the inter-slat spacing diminishes from 10 mm to 3 mm in the translucent state.
(2) In the clear state, the solar absorption of TT PS-TIM peaks at an incident angle of 60°. The slat interval seems to exert a minimal effect on the solar absorption per slat in the clear state. This implies that configurations with reduced slat intervals, due to their augmented slat count, possess an enhanced ability for solar energy absorption. In contrast, as the system transitions to the translucent state, there's a notable augmentation in solar absorption: systems with narrower slat intervals manifest greater absorption at lower solar incident angles, whereas those with wider intervals reflect increased absorption at elevated incident angles.
(3) The solar heat gain coefficient (SHGC) of TT PS-TIM decreases as the solar incident angle rises, following a pattern similar to transmittance. In the clear state, larger slat intervals result in higher SHGC. The impact of slat intervals on the SHGC in the translucent state becomes more pronounced at solar incident angles less than 50°.
(4) A surge in solar absorption per slat in TT PS-TIM corresponds to a reduction in the necessary average surface temperature of the glass, facilitating the transition of TT PS-TIM to its translucent state. With a 10 mm slat interval, the threshold average surface temperature of the glass displays a decrement of 0.3 °C for each incremental slat solar absorption from 0 to 60 W/m^2. This diminishing trend is accentuated with wider slat intervals, registering reductions of 0.5 °C and 1.3 °C at 7 mm and 5 mm intervals respectively. The zenith of this reduction, a remarkable 4.9 °C, is achieved with the most condensed slat interval of 3 mm.
(5) Employing Ray-tracing and Computational Fluid Dynamics (CFD) numerical simulations, accurate predictions of the thermal performance, switching states, and consequent building energy implications of TT PS-TIM have been conducted. When compared with conventional Double Glazing (DG) systems, TT PS-TIM showcases superior thermal performance, evidenced by over a 30 % reduction in heat gain during summer and approximately a 20 % reduction in heat loss during winter. Particularly, in this study, configurations with smaller slat intervals demonstrate a superior potential for energy conservation, underlining the effectiveness of TT PS-TIM as an energy-efficient solution.

This investigation presented a series of TT PS-TIM window designs for potential use in building applications, demonstrating their varying performance characteristics. Notably, the variant featuring a smaller slat interval emerged as the optimal choice for energy-saving purposes. The scope of this research was confined to forecasting the thermal performance of the TT PS-TIM system, providing a comprehensive model that will be instrumental for future energy consumption projections.

CRediT authorship contribution statement

Yang Ming: Conceptualization, Data curation, Formal analysis, Methodology, Writing – original draft. **Yanyi Sun:** Writing – review & editing, Methodology, Supervision. **Xin Liu:** Writing – review & editing. **Xiao Liu:** Writing – review & editing. **Yupeng Wu:** Conceptualization, Funding acquisition, Supervision, Writing – review & editing, Project administration, Resources.

Declaration of competing interest

The authors declare that they have no known competing financial interests or personal relationships that could have appeared to influence the work reported in this paper.

Data availability

No data was used for the research described in the article.

Acknowledgement

This work was supported by the Engineering and Physical Sciences Research Council, UK [grant number EP/S030786/1] and was supported by RAEng, UK [grant number TSP2021\100194].

References

[1] Alqahtani, et al., Development of affordable hot box calorimeter to determine the U-value of inhomogeneous building material, J. Mater. Res. Technol. 25 (2023) 6492–6502.
[2] Sun, et al., Numerical investigation of a smart window system with thermotropic Parallel Slat Transparent Insulation Material for building energy conservation and daylight autonomy, Build. Environ. 203 (2021) 108048.
[3] Nishikawa, et al., Experimental and numerical study of heat transfer from a window with an internal Venetian blind, Energ. Build. 223 (2020) 110128.

[4] Tao, et al., Impacts of thermo-optical properties on the seasonal operation of thermochromic smart window, Energ. Conver. Manage. 252 (2022) 115058.
[5] Zheng, et al., Effect of interior venetian blinds on natural convective heat exchange at a full-scale window glazing, Appl. Therm. Eng. 219 (2023) 119462.
[6] Yang, et al., Comprehensive performance evaluation of double-glazed windows containing hybrid nanoparticle-enhanced phase change material, Appl. Therm. Eng. 223 (2023) 119976.
[7] Kou, et al., Improved window energy efficiency with thermal insulating polymer-air multilayer, Appl. Therm. Eng. 191 (2021) 116890.
[8] Zhang, et al., Experimental investigation and dynamic modeling of a triple-glazed exhaust air window with built-in venetian blinds in the cooling season, Appl. Therm. Eng. 140 (2018) 73–85.
[9] Cannavale, et al., Energy savings due to building integration of innovative solid-state electrochromic devices, Appl. Energy 225 (2018) 975–985.
[10] Aburas, et al., Thermochromic smart window technologies for building application: a review, Appl. Energy 255 (2019) 113522.
[11] Wong and Chan, Smart glass and its potential in energy savings, J. Energy Res. Technol. 136 (1) (2014).
[12] Cao, et al., Sunlight-driven photo-thermochromic smart windows, Solar Rrl 2 (4) (2018) 1700219.
[13] Wang, Runnerstrom, and Milliron, Switchable materials for smart windows. 2016.
[14] Cui, et al., Thermochromic VO2 for energy-efficient smart windows, Joule 2 (9) (2018) 1707–1746.
[15] Zhang, et al., Thermochromic VO2 thin films: solution-based processing, improved optical properties, and lowered phase transformation temperature, Langmuir 26 (13) (2010) 10738–10744.
[16] A. Casini, dynamic windows for buildings: a review, Renew. Energy 119 (2018) 923–934.
[17] Long and Ye, Nano-based chromogenic technologies for building energy efficiency, in Start-Up Creation. 2016, Elsevier. p. 213-236.
[18] Lee, et al., An empirical study of a full-scale polymer thermochromic window and its implications on material science development objectives, Solar Energy Mater. Solar Cells **116** (2013) 14-26.
[19] Karlessi, et al., Development and testing of thermochromic coatings for buildings and urban structures. Solar Energy 83(4) (2009) 538-551.
[20] Seeboth, Ruhmann, Mühling, Thermotropic and thermochromic polymer based materials for adaptive solar control, Materials **3**(12) (2010) 5143–5168.
[21] Yang, et al., Performance analyses of building energy on phase transition processes of VO2 windows with an improved model. Appl. Energy 159 (2015) 502-508.
[22] Ke, et al., Smart windows: electro-, thermo-, mechano-, photochromics, and beyond, Adv. Energy Mater. 9 (39) (2019) 1902066.
[23] Li, et al., Durable and controllable smart windows based on thermochromic hydrogels, ACS Appl Mater Interfaces 12 (37) (2020) 42193–42201.
[24] Zhou, et al., Hydrogel smart windows, J. Mater. Chem. A 8 (20) (2020) 10007–10025.
[25] Haq, Su, and Wang, Mechanical properties of PNIPAM based hydrogels: A review. Mater Sci Eng C Mater Biol Appl, 2017. **70**(Pt 1): p. 842-855.
[26] Jian, Modeling and simulation for the optimal switching temperature of double-glazed thermotropic window. 2010 the 2nd International Conference on Industrial Mechatronics and Automation, 2010.
[27] D. Gladen, S. Mantell, of thermotropic materials for overheat protection of polymer absorbers, Sol. Energy 104 (2014) 42–51.
[28] Granqvist and Wittwer, Materials for solar energy conversion: an overview, Sol. Energy Mater. Sol. Cells 54 (1) (1998) 39–48.
[29] Inoue, Ichinose, and Ichikawa, Thermotropic glass with active dimming control for solar shading and daylighting. Energy Build. 40(3) (2008) 385–393.
[30] Watanabe, Intelligent window using a hydrogel layer for energy efficiency, Sol. Energy Mater. Sol. Cells 54 (1) (1998) 203–211.
[31] W. Paneri, T. Burek, insulation materials: An overview on past, present and future developments, Sol. Energy 184 (2019) 59–83.
[32] Dowson. *Novel retrofit technologies incorporating silica aerogel for lower energy buildings*. 2012.
[33] Kaushika, Sumathy, Solar transparent insulation materials: a review, Renew. Sustain. Energy Rev. 7 (4) (2003) 317–351.
[34] Wittwer and Platzer, Transparent thermal insulation materials and systems: State of the art and potential for the future, High Temperatures-High Pressures 32 (2000) 143–158.
[35] Wong, Eames, Perera, A review of transparent insulation systems and the evaluation of payback period for building applications, Solar Energy 81(9) (2007) 1058-1071.
[36] Arulanantham, Reddy, Kaushika, Solar gain characteristics of absorber-parallel transparent insulation materials. Energy Convers. Manage. 39(15) (1998) 1519-1527.
[37] Sun, et al., Glazing systems with Parallel Slats Transparent Insulation Material (PS-TIM): Evaluation of building energy and daylight performance, Energ. Build. 159 (2018) 213–227.
[38] Sun, et al., Thermal evaluation of a double glazing façade system with integrated Parallel Slat Transparent Insulation Material (PS-TIM), Build. Environ. 105 (2016) 69–81.
[39] Platzer, Transparent insulation materials: a review. in Optical Materials Technology for Energy Efficiency and Solar Energy Conversion XIII, 1994. SPIE.
[40] Sun, et al., Energy and daylight performance of a smart window: Window integrated with thermotropic parallel slat-transparent insulation material, Appl. Energy 293 (2021) 116826.
[41] W.u. Sun, A. Wilson, of the daylight performance of a glazing system with Parallel Slat Transparent Insulation Material (PS-TIM), Energ. Build. 139 (2017) 616–633.
[42] Ming, et al., Optical evaluation of a smart transparent insulation material for window application, Energy Convers. Manage.: X 16 (2022) 100315.
[43] Zhuang, et al., 3D ordered macroporous VO2 thin films with an efficient thermochromic modulation capability for advanced smart windows. Adv. Opt. Mater. 7(22) (2019) 1900600.
[44] Li, et al., Z-scheme g-C3N4@CsxWO3 heterostructure as smart window coating for UV isolating, Vis penetrating, NIR shielding and full spectrum photocatalytic decomposing VOCs, Appl Catal B 229 (2018) 218–226.
[45] Liang, et al., Enhanced visible and tunable infrared transmittance of W-doped VO2/SiO2/PVP composite films for smart windows, Opt. Mater. 121 (2021) 111485.
[46] Wei, et al., Thermal-responsive PNIPAm-acrylic/Ag NRs hybrid hydrogel with atmospheric window full-wavelength thermal management for smart windows, Sol. Energy Mater. Sol. Cells 206 (2020) 110336.
[47] Piccolo, Thermal performance of an electrochromic smart window tested in an environmental test cell, Energ. Buildings 42 (9) (2010) 1409–1417.
[48] Ciampi, et al., Thermal model validation of an electric-driven smart window through experimental data and evaluation of the impact on a case study, Build. Environ. 181 (2020) 107134.
[49] Xamán, et al., Thermal evaluation of a Room coupled with a Double Glazing Window with/without a solar control film for Mexico, Appl. Therm. Eng. 110 (2017) 805–820.
[50] Tao, et al., CFD analysis of environmental impacts on a thermochromic smart window, Energ. Buildings 263 (2022) 112027.
[51] L. Jin, N. Liang, analysis on the thermal performance of PCM-integrated thermochromic glazing systems, Energ. Build. 257 (2022) 111734.
[52] Xamán, et al., Computational fluid dynamics for thermal evaluation of a room with a double glazing window with a solar control film, Renew. Energy 94 (2016) 237–250.
[53] Demanega, et al., CFD and ray tracing to evaluate the thermal performance of Complex Fenestration Systems. In Proceedings of the 2018 Building Simulation and Optimization Conference in Cambridge, 2018.
[54] Wu, et al., Smart solar concentrators for building integrated photovoltaic façades, Sol. Energy 133 (2016) 111–118.
[55] M.R. Zahri, R.T. Pakhuruddin, of Perovskite thin films for solar windows, Key Eng. Mater. 946 (2023) 81–86.
[56] S. Bush, Loutzenhiser, Pairing directional solar inputs from ray tracing to solar receiver/reactor heat transfer models on unstructured meshes: development and case studies, J. Sol. Energy Eng. 143 (3) (2020).
[57] Lee, et al., A dual-responsive nanocomposite toward climate-adaptable solar modulation for energy-saving smart windows, ACS Appl Mater Interfaces 9 (7) (2017) 6054–6063.
[58] Shadmehri, et al., Numerical simulation of a concentrating photovoltaic-thermal solar system combined with thermoelectric modules by coupling Finite Volume and Monte Carlo Ray-Tracing methods, Energ. Conver. Manage. 172 (2018) 343–356.
[59] L. Butti, et al., Effect of surface material properties and operating conditions on the heat flux and temperature distributions in the cavity receiver of a solar-dish-coupled biomass gasification reactor, Energ. Conver. Manage. 244 (2021) 114303.
[60] Liu and Wu, Monte-Carlo optical model coupled with Inverse Adding-Doubling for Building Integrated Photovoltaic smart window design and characterisation, Sol. Energy Mater. Sol. Cells 223 (2021) 110972.
[61] 15099, Thermal performance of windows, doors and shading devices – Detailed calculations. 2003.
[62] Baenas and Machado, On the analytical calculation of the solar heat gain coefficient of a BIPV module, Energ. Buildings 151 (2017) 146–156.
[63] DepartmentofEnergy, *EnergyPlus EngineeringReference*. 2022.